Millennial-scale variability in Red Sea circulation in response to Holocene insolation forcing

Gabriele Trommer,[1,2] Michael Siccha,[1,3] Eelco J. Rohling,[4] Katherine Grant,[4]
Marcel T. J. van der Meer,[5] Stefan Schouten,[5] Christoph Hemleben,[1] and Michal Kucera[1]

Received 15 July 2009; revised 4 March 2010; accepted 1 April 2010; published 17 July 2010.

[1] In order to assess how insolation-driven climate change superimposed on sea level rise and millennial events influenced the Red Sea during the Holocene, we present new paleoceanographic records from two sediment cores to develop a comprehensive reconstruction of Holocene circulation dynamics in the basin. We show that the recovery of the planktonic foraminiferal fauna after the Younger Dryas was completed earlier in the northern than in the central Red Sea, implying significant changes in the hydrological balance of the northern Red Sea region during the deglaciation. In the early part of the Holocene, the environment of the Red Sea closely followed the development of the Indian summer monsoon and was dominated by a circulation mode similar to the current summer circulation, with low productivity throughout the central and northern Red Sea. The climatic signal during the late Holocene is dominated by a faunal transient event centered around 2.4 ka BP. Its timing corresponds to that of North Atlantic Bond event 2 and to a widespread regionally recorded dry period. This faunal transient is characterized by a more productive foraminiferal fauna and can be explained by an intensification of the winter circulation mode and high evaporation. The modern distribution pattern of planktonic foraminifera, reflecting the prevailing circulation system, was established after 1.7 ka BP.

Citation: Trommer, G., M. Siccha, E. J. Rohling, K. Grant, M. T. J. van der Meer, S. Schouten, C. Hemleben, and M. Kucera (2010), Millennial-scale variability in Red Sea circulation in response to Holocene insolation forcing, *Paleoceanography*, *25*, PA3203, doi:10.1029/2009PA001826.

1. Introduction

[2] The climate of the Holocene is known to have been affected by global persistent millennial-scale variability [*Denton and Karlén*, 1973; *Kennett and Ingram*, 1995; *O'Brien et al.*, 1995; *Alley et al.*, 1997; *Bond et al.*, 1997; *Bianchi and McCave*, 1999; *Rohling et al.*, 2002; *Mayewski et al.*, 2004; *Rohling and Pälike*, 2005]. This variability has been considered as periodic and attributed to solar variation [*Bond et al.*, 2001] and also as irregular and attributable to unique events such as the drainage of proglacial lakes [*Barber et al.*, 1999]. Evidence for millennial-scale events has been found in climate records of the eastern Mediterranean Sea [*Casford et al.*, 2001; *Rohling et al.*, 2002], the Middle East [*Cullen et al.*, 2000; *Parker et al.*, 2006], the Arabian Sea [*Berger and von Rad*, 2002; *Gupta et al.*, 2003] and the Gulf of Aqaba in the Red Sea [*Lamy et al.*, 2006]. Until now, relatively little is known about Holocene paleoclimate variation in the Red Sea itself, apart from a distinct event at around 4.2 ka BP that has been attributed to increased deep water ventilation due to increased aridity [*Almogi-Labin et al.*, 2004; *Arz et al.*, 2006; *Edelman-Furstenberg et al.*, 2009].

[3] The Red Sea has received an increasing amount of attention as an important archive of sea level change [*Rohling et al.*, 1998; *Arz et al.*, 2003a, 2003b; *Siddall et al.*, 2003, 2004; *Arz et al.*, 2007]. Sea level fluctuations clearly dominated the conditions in the basin on glacial-interglacial timescales [*Locke and Thunell*, 1988; *Hemleben et al.*, 1996; *Almogi-Labin et al.*, 1998; *Fenton et al.*, 2000] as well as during the glacials [*Rohling et al.*, 2008a] and interglacials [*Rohling et al.*, 2008b]. However, comparatively little information exists about the Red Sea circulation variability during interglacial periods, when sea level remained relatively stable. Since the basin is and always has been strongly isolated from the open ocean, large sensitivity to signals of regional climatic variability other than sea level change should be expected during relatively stable interglacials. Thus, the Red Sea should be a good location to investigate regional climate trends and events during the Holocene sea level highstand.

[4] Circulation and productivity in the Red Sea are controlled by the water exchange between the Red Sea and the Indian Ocean, which is affected by the dominant wind systems. Because the Red Sea is located between the westerlies-dominated climate system of the Mediterranean

[1]Institute of Geosciences, University of Tübingen, Tübingen, Germany.
[2]Europole Mer, European Institute for Marine Studies, Technopole Brest-Iroise, Plouzane, France.
[3]Laboratoire des Bio-Indicateurs Actuels et Fossiles, UFR Sciences, Angers, France.
[4]National Oceanography Centre, University of Southampton, Southampton, UK.
[5]Department of Marine Organic Biogeochemistry, Royal Netherlands Institute for Sea Research, Den Burg, Netherlands.

0883-8305/10/2009PA001826

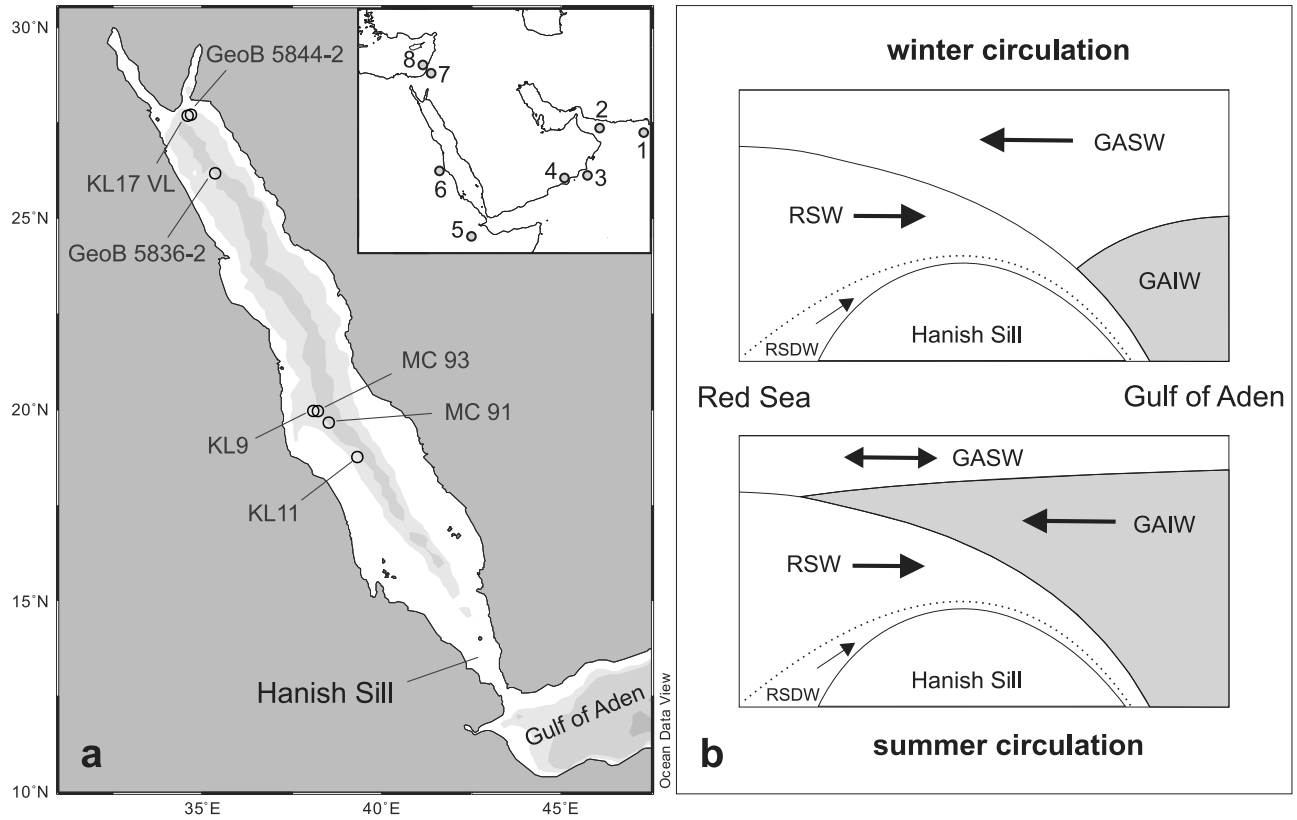

Figure 1. (a) Map (Ocean Data View (R. Schlitzer, 2007; available at http://odv.awi.de)) showing the Red Sea with locations of sediment cores in this study (KL17 VL and KL9), as well as previously published records from GeoB 5844-2 [*Arz et al.*, 2003a], GeoB 5836-2 [*Arz et al.*, 2006], KL11 [*Almogi-Labin et al.*, 1991; *Schmelzer*, 1998], and MC93 and MC91 [*Edelman-Furstenberg et al.*, 2009]. The inset map displays locations of other climate records discussed in the text, including Arabian Sea sediment cores, 1 [*Doose-Rolinski et al.*, 2001; *Lückge et al.*, 2001; *Berger and von Rad*, 2002; *von Rad et al.*, 2006], 2 [*Cullen et al.*, 2000], and 3 [*Gupta et al.*, 2003]; Qunf cave speleothem, 4 [*Fleitmann et al.*, 2003]; Lake Abhé and Ziway-Shala, 5 [*Gasse and Van Campo*, 1994]; Red Sea Hills, 6 [*Mawson and Williams*, 1984]; Soreq cave speleothem, 7 [*Bar-Matthews et al.*, 1999]; and Mediterranean sediment core, 8 [*Schilman et al.*, 2001]. (b) Modified exchange scheme over the Hanish Sill [*Smeed*, 1997; *Siddall et al.*, 2004]. See text for explanation and abbreviations.

and the Indian Monsoon, fluctuations of these two climate systems during interglacials influence the oceanography of the basin. The influence of Mediterranean climate fluctuations has been previously inferred for the early Holocene of the northern Red Sea [*Arz et al.*, 2003a; *Legge et al.*, 2006], but the influence of the Indian Monsoon system on the Red Sea remains to be clarified. It is well established that the Indian Monsoon strength affects the hydrography of the southern and central Red Sea [*Almogi-Labin et al.*, 1991; *Hemleben et al.*, 1996], but the effects on the entire circulation system and its sensitivity to climate fluctuations are still unknown.

[5] Using two new sediment core records combined with existing data, we aim to investigate which rapid climate events and climate trends are recorded in Holocene Red Sea sediments and by which mechanisms they affected the basin. To this end, we use newly developed micropaleontological and geochemical proxy approaches for the Red Sea to reconstruct surface water productivity based on planktonic foraminifera [*Siccha et al.*, 2009] and sea surface temperature (SST) based on archaeal membrane lipids [*Trommer et al.*, 2009]. An analysis of these and other proxies is used to develop comprehensive scenarios of circulation regimes of the Red Sea and their relationships with the Indian Monsoon and Mediterranean climate system.

2. Red Sea Oceanography and Paleoceanography

[6] The Red Sea (Figure 1a) is a desert-enclosed, narrow basin of about 2000 km length, with a maximum width of about 350 km. The only connection of the basin to the open ocean is through Bab el Mandab in the south, leading to the Gulf of Aden in the Indian Ocean. The Red Sea circulation system follows an anti-estuarine pattern and is driven by thermohaline forcing [*Eshel et al.*, 1994; *Sofianos and Johns*, 2002]. Monsoon-controlled seasonal winds affect

only the surface waters in the southern part of the basin [*Eshel et al.*, 1994; *Sofianos et al.*, 2002] and northward flowing Gulf of Aden surface waters pass through a seasonal array of boundary currents with permanent and semi-permanent gyres [*Quadfasel and Baudner*, 1993; *Biton*, 2006]. High evaporation rates that reach up to 2.1 m/a result in highly saline (40.5) and relatively cool (24.5°C) surface water conditions in the north that induce deep-water formation in the northern Red Sea [*Sofianos et al.*, 2002]. The resultant Red Sea deep water (RSDW) has a uniform salinity of 40.6 and a temperature of 21.6°C [*Morcos*, 1970] (see also M. E. Conkright et al., *World Ocean Atlas 2001*, 2001; available at http://odv.awi.de/en/data/ocean/world_ocean_atlas_2001/). The circulation pattern of deep water masses in the basin and volumetric differences between different modes of deep water formation remain to be fully established [*Cember*, 1988; *Eshel et al.*, 1994; *Woelk and Quadfasel*, 1996; *Eshel and Naik*, 1997; *Manasrah et al.*, 2004].

[7] On the basin side, north of Bab el Mandab, the Hanish Sill with only 137 m depth is the critical point for water exchange between the Red Sea and the Gulf of Aden, and seasonal climatic differences cause an alternation between seasonally distinct circulation regimes [*Patzert*, 1974; *Murray and Johns*, 1997; *Smeed*, 1997; *Siddall et al.*, 2002; *Smeed*, 2004]. During October to April (Indian NE Monsoon) the exchange is two-layered; surface water from the Gulf of Aden (GASW) enters the Red Sea, while subsurface Red Sea Water (RSW) flows out of the basin (Figure 1b). From May to September (Indian SW Monsoon) the exchange pattern in the strait is three-layered. Above the deepest outflow layer of Red Sea Water, an intermediate layer of nutrient-rich water from the upwelling regions of the Gulf of Aden (GAIW) [*Smeed*, 1997] intrudes into the Red Sea (Figure 1b). At the surface, a thin layer of surface water leaves the Red Sea.

[8] During the Indian summer SW Monsoon, upwelling of nutrient-rich deep water takes place in the Gulf of Aden. Intrusion of these nutrient-enriched waters into the Red Sea increases productivity in the very southern sector of the basin (south of 14° N), with chlorophyll *a* concentrations markedly higher than those in winter (up to 2 mg/m^3 (G. C. Feldman and C. R. McClain, Ocean Color Web, SeaWIFS/Chlorophyll a concentration, 07/2002–06/2006, NASA Goddard Space Flight Center, 2006; available at http://oceancolor.gsfc.nasa.gov)), whereas the central and northern Red Sea remain oligotrophic with low chlorophyll *a* values of 0.1–0.2 mg/m^3. Productivity maxima in these latter regions occur during winter [*Veldhuis et al.*, 1997], but even then with very low chlorophyll *a* concentrations around 0.3 mg/m^3 (G. C. Feldman and C. R. McClain, online data, 2006). This winter productivity is unlikely to be caused directly by inflowing waters from the Gulf of Aden, which contain less nutrients than the summer inflow [*Souvermezoglou et al.*, 1989] but is most likely related to convective mixing in the water column [*Clifford et al.*, 1997; *Smeed*, 1997; *Veldhuis et al.*, 1997]. In the northern Red Sea, mixing of the water column occurs in association with deep water formation, which takes place almost exclusively during the winter [*Cember*, 1988; *Woelk and Quadfasel*, 1996; *Manasrah et al.*, 2004].

[9] It has been shown previously that pteropod assemblages can be used to reconstruct changes in the stratification of the mesopelagic layer [e.g., *Almogi-Labin*, 1982; *Almogi-Labin et al.*, 1991, 1998]. Studies of calcareous nannofossil [*Legge et al.*, 2006, 2008] and diatom assemblages [*Seeberg-Elverfeldt et al.*, 2005] indicate sensitive responses of the plankton community in the Red Sea to atmospheric forcing and the coupling of the northern Red Sea and the North Atlantic realm. A strong spatial gradient in the recent distribution of planktonic foraminifera in the basin [*Auras-Schudnagies et al.*, 1989] and a strong response of foraminiferal faunas to salinity changes during sea level lowstands [*Fenton et al.*, 2000] indicate that planktonic foraminiferal assemblages could serve as an efficient proxy for surface water properties in the basin during interglacials. Until recently, however, little was known about the nature of the signal recorded in planktonic foraminiferal assemblages of the Red Sea and earlier studies of planktonic foraminifer assemblages in the basin either focused on glacial-interglacial timescales [*Fenton et al.*, 2000], were of low resolution [*Berggren and Boersma*, 1969; *Fenton et al.*, 2000] or covered short timescales [*Edelman-Furstenberg et al.*, 2009]. Recently, we have developed the first transfer function approach on planktonic foraminiferal faunal assemblages for the Red Sea and found that the recent faunal distribution and variation during interglacials are predominantly recording changes in surface ocean productivity [*Siccha et al.*, 2009]. Such productivity reconstructions will help to understand the circulation system of the Red Sea, since productivity is primarily controlled by different circulation regimes in the northern and southern Red Sea (see above).

3. Material and Methods

3.1. Core Material

[10] In order to investigate changes in the circulation of the Red Sea throughout the Holocene, surface ocean properties were reconstructed by multiple proxies in two sediment cores. The cores are situated in oceanographic key areas of the Red Sea: the deep water formation area in the north, and the monsoon influenced central Red Sea. The core material was recovered during *RV Meteor* cruises M5/2 (piston core KL9, 19°57.6′N, 38°06.3′E) and M31/2 (trigger core KL17 VL, 27°41.1′N, 34°35.76′E) (Figure 1a) and stored in the Tübingen/Sand core repository.

[11] The analyzed section for KL9 spans the top 90 cm of the core. Directly below, we find a strong decrease in planktonic foraminiferal numbers down to an interval of cemented sediments between 91 and 168 cm [see also *Rohling et al.*, 2008a]. Such cemented intervals developed during glacial sea level lowstands in the Red Sea due to post-depositional carbonate production [*Brachert*, 1999]. The analyzed section in KL17 VL spans the top 129 cm. Below 97 cm numbers of planktonic foraminifera are lower than 50 per gram sediment (except for one sample at 104.5 cm depth), which is typical for glacial periods in the Red Sea, with salinity values exceeding the tolerance limits of foraminifera species [*Hemleben et al.*, 1996; *Fenton et al.*, 2000]. This study focuses on the establishment of, and

Table 1. Conventional and Calibrated ^{14}C AMS Dates (ΔR of 170 years) of Red Sea Cores KL17 VL, KL9, and KL11[a]

Mean Depth (cm)	Conventional Age (yrs BP)	± Error (yrs)	Calibrated Age Range (2 σ)	Mean Calibrated Age (a BP)	Faunal Age (a BP)
			Core KL17 VL		
0.5	520	25	0–234[b]	117	228
7.5	1495	30	712–1023	868	1009
21.5	3455	30	2926–3319	3123	3317
92.5	10340	50	10925–11341	11133	10912[c]
			Core KL9		
2.25	1315	25	562–852	707	578
24.25	3260	25	2728–3054	2891	2372[c]
30.25	3465	25	2942–3324	3133	3045
50.25	4950	30	4856–5258	5057	5233
60.25	6595	35	6732–7125	6929	6753
84.25	8955	40	9270–9603	9437	9566
			Core KL11		
27.5	2895	65	2241–2704	2473	2473
51.5	6005	75	5996–6452	6224	6135
78.5	8700	80	8931–9434	9183	9363
82.5	9650	85	10140–10556	10348	10171
86	11250	95	12333–12879	12606	12333

[a]Core data from *Schmelzer* [1998]. The final age model refers to the faunal correlated and corrected age (= faunal age) of the dated samples.
[b]ΔR of 70 was used.
[c]More than 2 σ range deviation in the final age model.

subsequent variations in, the faunas as stable populations developed roughly after the Younger Dryas.

[12] Chronology of the core sections is based on ^{14}C accelerator mass spectrometry (AMS) radiocarbon dating of hand-picked tests of the planktonic foraminifer *Globigerinoides sacculifer* (250–315 μm size fraction) (Table 1). Analyses were performed at the Leibniz Labor für Altersbestimmung und Isotopenforschung in Kiel, Germany. Calibration of AMS-datings was performed using the software program *Calib 5.0.1* [*Stuiver and Reimer*, 1993], using the *Marine04* calibration [*Hughen et al.*, 2004] (see details in section 4.4).

3.2. Planktonic Foraminiferal Assemblages

[13] Planktonic foraminiferal faunal composition was investigated in resolutions of at least 4 cm in KL 17 VL, and 2 cm in KL 9. The resolution was increased to 1 cm intervals in both cores where a faunal transient event was observed. All samples were dried, weighed, washed over a >63 μm mesh, dry sieved over a > 150 μm mesh, and split with an *ASC Scientific* microsplitter. For each sample an aliquot containing at least 300 specimens of planktonic foraminifera was counted and identified to species level, following the taxonomy of *Hemleben et al.* [1989]. The faunal data of each sample were purged of species that never reached 1% relative abundance in order to avoid the influence of rare species which might or might not have been recorded by chance. The purged data were then recalculated to 100%. None of the samples showed any signs of carbonate dissolution.

3.3. Stable Isotope Analyses

[14] Carbon and oxygen isotope measurements were performed for both cores in at least 4 cm resolution. For each sample, approximately 10–15 tests of the planktonic foraminifer *Globigerinoides ruber* were hand-picked from the size fraction 250–315 μm and ultrasonically cleaned. The isotopic composition of the calcite tests was measured with a *Europa Scientific Geo2020* mass spectrometer at the National Oceanography Centre, Southampton (NOCS, UK). Values are reported in conventional delta notation relative to the international V-PDB standard. External precision is monitored using blind standards within each run, and was better than 0.06‰ for both oxygen and carbon.

[15] Nitrogen stable isotope analyses of bulk organic matter were performed in 5 cm intervals for KL 9 to detect changes in primary productivity. For each sample, 40–50 mg of homogenized, decalcified and freeze-dried sediment was measured with a *Thermofinnigan Delta Plus* isotope ratio mass spectrometer at the Royal Netherlands Institute for Sea Research (Den Burg, Texel, The Netherlands). Nitrogen isotope abundances are given in conventional delta notation. The nitrogen isotopic composition was calibrated against laboratory standards glycine and acetanilide. Reproducibility of the isotopic analysis was determined by duplicate analysis, which yielded pooled standard errors of <0.2‰.

3.4. Color Scanner Measurements

[16] For color reflectance measurements, core halves were smoothed to ensure an even surface and analyzed at 0.5 mm resolution using a *DMT Slab-CoreScan© Color* scanner in Tübingen. Raw data were manually adjusted to eliminate reflectance artifacts that resulted from small cracks in the dried-out sediment.

3.5. Transfer Functions

[17] Abundance counts of planktonic foraminifera have been used to reconstruct primary productivity following the approach developed by *Siccha et al.* [2009]. We here employ two transfer function methods, the weighted averaging partial least square regression (WA-PLS [*ter Braak and Juggins*, 1993]) and the artificial neural networks technique (ANN [*Malmgren and Nordlund*, 1997]), to convert foraminiferal assemblage census counts into absolute values of surface chlorophyll *a* concentrations, following the procedures described by *Siccha et al.* [2009]. Reconstruction uncertainties lie at ± 0.1 mg/m^3 chlorophyll *a*.

3.6. TEX_{86} and BIT Analyses

[18] To reconstruct sea surface temperatures and soil organic matter input we determined the TEX_{86} and BIT proxies, respectively, based on the analysis of glycerol dialkyl glycerol tetraethers (GDGTs) [*Trommer et al.*, 2009]. For this, sediment samples were taken in 10 cm resolution from KL17 VL and at least 8 g of sediment were freeze-dried and homogenized by mortar and pestle for lipid analyses. Extraction of the homogenized sediments was carried out with an *Accelerated Solvent Extractor 200* (ASE 200, DIONEX) using dichloromethane (DCM)/methanol (MeOH) 9:1 (v:v) at 100°C and 7.6 × 10^6 Pa, and polar fractions were isolated from the obtained extracts following *Trommer et al.* [2009]. The polar fractions, containing the required GDGTs were analyzed by high performance liquid

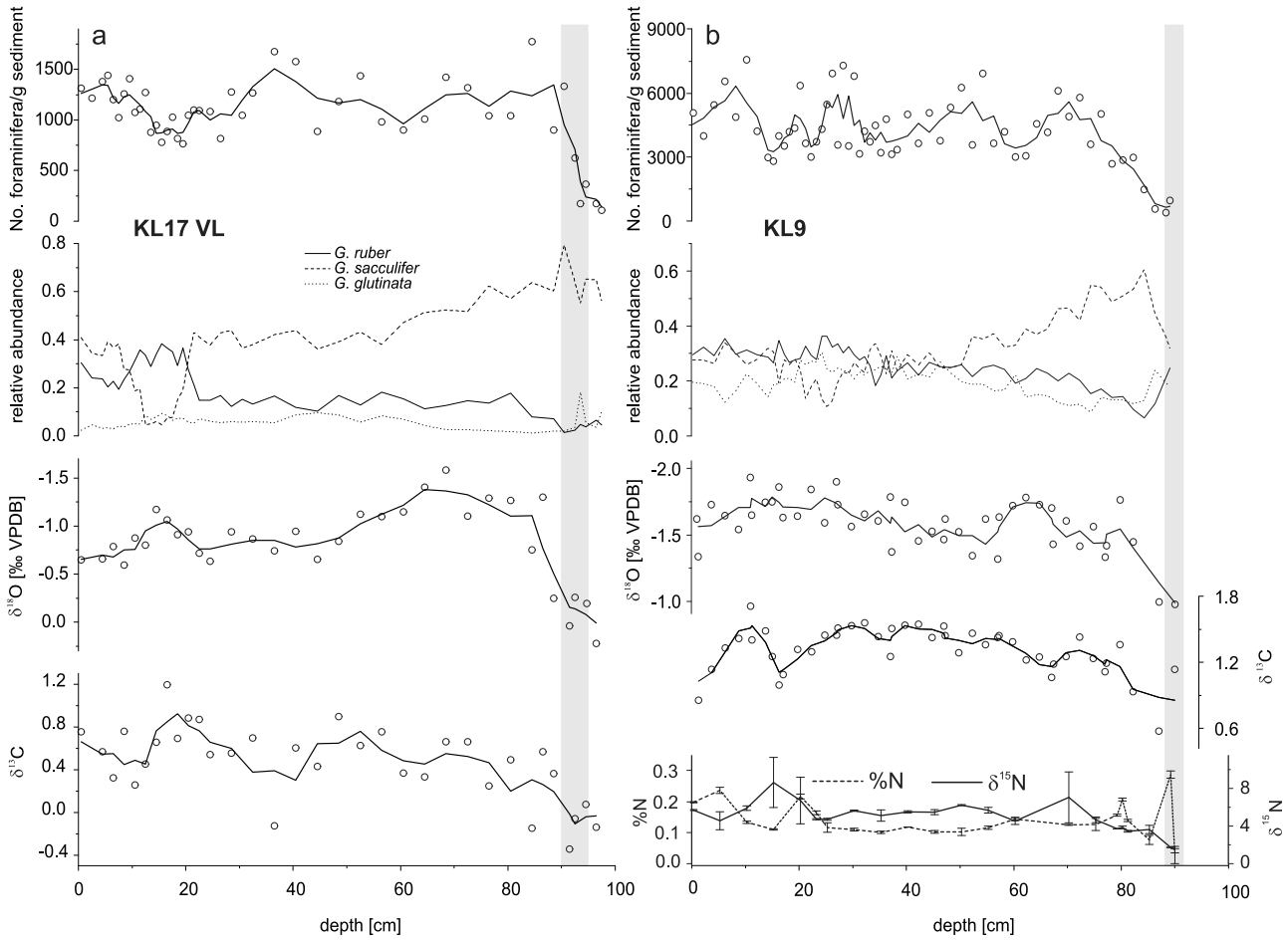

Figure 2. Faunal and stable isotope data of (a) core KL17 VL and (b) core KL9. Number of foraminifera/g sediment (circles: raw data, solid line: 3p running mean); relative abundances of the dominant foraminifera species *G. ruber*, *G. sacculifer*, and *G. glutinata*; and oxygen and carbon stable isotopes (circles: raw data, solid line: 3p running mean). Nitrogen stable isotopes (% versus air) and nitrogen content (%) in sediments of KL9 (error bars: standard deviation of measurements). Light gray bars indicate the sapropel position.

chromatography (HPLC) atmospheric pressure chemical ionization (APCI) mass spectrometry (MS) with an *Agilent 1100 series LC MSD* series instrument equipped with an auto-injection system and *HP-Chemstation* software (for details see *Hopmans et al.* [2000] and *Schouten et al.* [2007]). GDGTs were detected with selected ion monitoring (SIM) of their protonated molecules [M + H] + (dwell time = 234 ms), quantified by manual integration of peak areas of the mass chromatograms and further used in the calculation of the TEX_{86} following *Schouten et al.* [2002]:

$$TEX_{86} = ([GDGT\ 2] + [GDGT\ 3] + [GDGT\ 4'])/([GDGT\ 1] + [GDGT\ 2] + [GDGT\ 3] + [GDGT\ 4']) \quad (1)$$

GDGTs 1–3 are GDGTs with 1–3 cyclopentane moieties, respectively, and GDGT 4′ represents the regio-isomer of crenarchaeol (see *Schouten et al.* [2002] for structures). Temperatures were calculated using the northern Red Sea calibration of *Trommer et al.* [2009]:

$$T = (TEX_{86} + 0.09)/0.035 \quad (2)$$

In addition, the Branched versus Isoprenoid Tetraether (BIT) index was calculated following *Hopmans et al.* [2004], to describe the relative contribution of soil organic matter in marine environments [*Huguet et al.*, 2007; *Walsh et al.*, 2008]. Branched GDGT lipids are dominant in soils [*Weijers et al.*, 2006] and can therefore be used to determine the input of the soil-derived lipids in marine environments.

4. Results

4.1. Planktonic Foraminifera

[19] The abundance of planktonic foraminifera species has been determined in 58 samples from KL9 in the central Red Sea and 46 from KL17 VL in the northern Red Sea (Full

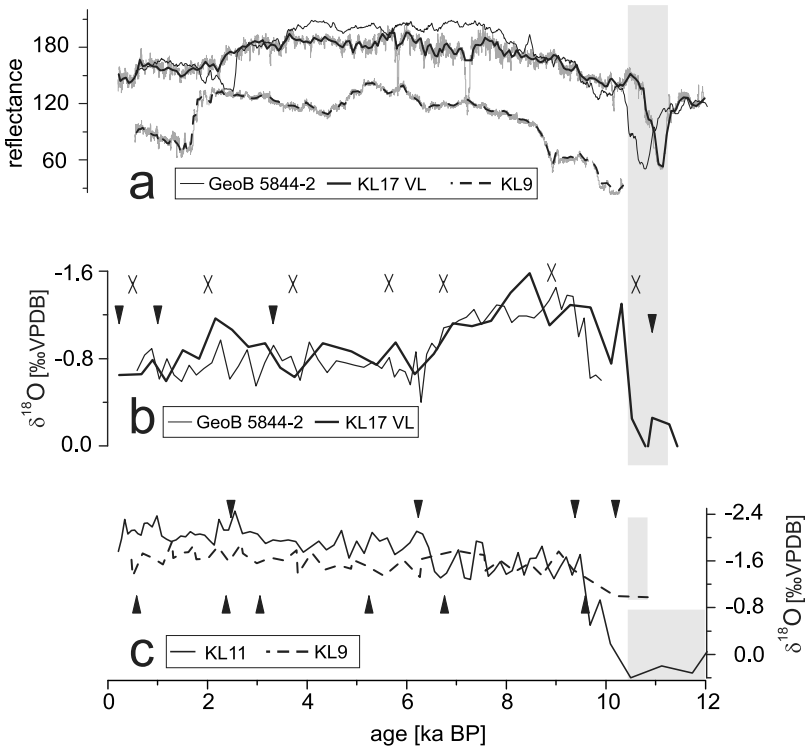

Figure 3. Age model comparison: plotted are (a) reflectance measurements of the cores GeoB 5844-2 [*Arz et al.*, 2003a], KL17 VL, and KL9 (5 mm resolution and running mean); (b) oxygen stable isotopes of the cores GeoB 5844-2 [*Arz et al.*, 2003a] (thin solid line, crosses: calibrated ^{14}C ages), and KL17 VL (bold solid line, downward triangles: ^{14}C ages corrected by tuning of faunal trends (= faunal age)), and (c) oxygen stable isotopes of cores KL11 [*Schmelzer*, 1998] (thin solid line, downward triangles: faunal age) and KL9 (bold dashed line, upward triangles: faunal age). Light gray bars indicate the sapropel position.

faunal data are presented in Data Sets S1 and S2).[1] A total of 19 species has been identified, but only seven species occurred frequently enough to account for more than 1% relative abundance of all samples per core: *Globigerinoides ruber* (white), *Globigerinoides sacculifer*, *Globigerinita glutinata*, *Globigerinella siphonifera*, *Globigerinella calida*, *Globoturborotalita tenella* and *Orbulina universa*. The three most abundant species, *Globigerinoides sacculifer*, *Globigerinoides ruber* and *Globigerinita glutinata* alone account for 76.4% (KL9) and 63.3% (KL17 VL) of the Holocene foraminiferal fauna, and show distinct and similar abundance patterns in both records.

[20] At the base of both Holocene records, total foraminiferal abundances per gram sediment are very low (Figure 2), but they increase to average Holocene levels within 10 cm (KL17 VL) and 20 cm (KL9), reflecting the re-establishment of stable planktonic foraminiferal faunas in the Red Sea after glacial high salinity conditions [*Fenton et al.*, 2000]. After this re-colonization phase, total foraminiferal abundances fluctuate around 10^3 (KL17 VL) and 4.5×10^3 (KL9) individuals per gram dry sediment.

[21] Relative abundances of the main species show an alternation between *G. sacculifer* and *G. ruber* as the dominant species in both records. In KL17 VL, dominance of *G. sacculifer* is maintained throughout the record, except around 15 cm, where *G. ruber* becomes the dominant species. In KL9, the dominance of *G. sacculifer* ends at around 50 cm, and the abundance of this species reaches a distinct minimum at around 25 cm. Abundances of *G. ruber* generally increase toward the top of both records and reach a temporary maximum at 15 cm in KL17 VL and 25 cm in KL9 (hereafter referred to as 'faunal transient'). In KL9 the abundance patterns of *G. glutinata* follow those of *G. ruber* until the end of the faunal transient, after which the abundance of *G. glutinata* decreases slightly. In KL17 VL, the abundance of *G. glutinata* remains very low, around 6%.

4.2. Stable Isotopes

[22] While the foraminiferal faunas of both cores show similar features, the oxygen isotope ratios display different trends (Figure 2). The δ^{18}O record of KL17 VL is very similar to that of nearby core GeoB 5844-2 [*Arz et al.*, 2003a] (Figure 3). The isotopic signal decreases steeply toward lighter values at the beginning of the record and maintains light values up to a depth level of 50 cm (Figure 2a). Furthermore, we observe a short-term excursion of ~0.3‰ to lighter values at around 15 cm. The oxygen isotope signal of KL9 shows a decreasing trend from the beginning until 65 cm

[1] Auxiliary materials are available at ftp://ftp.agu.org/apend/pa/2009pa001826.

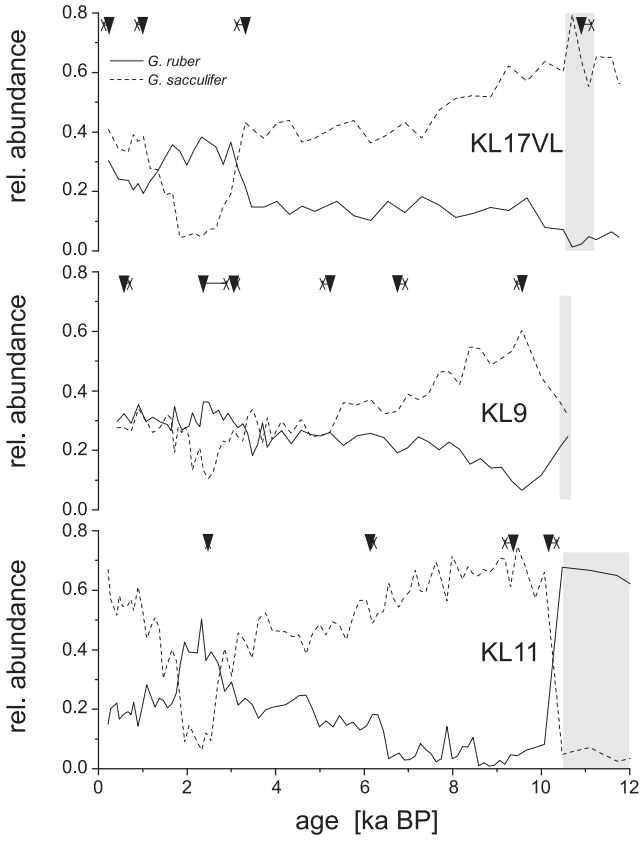

Figure 4. Age models of cores KL17 VL, KL9, and KL11 [*Schmelzer*, 1998] based on correlation of the foraminifera fauna (*G. sacculifer*, *G. ruber*) and ^{14}C AMS dates. Crosses: calibrated ^{14}C ages, triangles: ^{14}C ages corrected by tuning of faunal trends (= faunal age) (Table 1). Light gray bars indicate the sapropel position.

and fluctuates around −1.6‰ through the rest of the record (Figure 2b).

[23] The carbon isotope records of planktonic foraminifera (Figure 2) of both cores show an increasing trend in both absolute values and variability over the analyzed period, which is more pronounced in the northern Red Sea core KL17 VL. Toward the end of the records, a local maximum in δ^{13}C is observed around 20 cm in KL17 VL and 10 cm in KL9, respectively. The δ^{15}N of decalcified bulk sediment in KL9 increases in the first 15 to 20 cm and fluctuates around 5‰ for the rest of the record (Figure 2b). One single sample at 15 cm presents a heavier value of 8.5‰.

4.3. Sediment Properties

[24] The most prominent optical feature of KL17 VL and KL9 is a sapropel layer at the base of the analyzed core sections. While the sapropel in KL17 VL is clearly defined (see reflectance in Figure 3) and extends from 95 to 90 cm, the analyzed section of KL9 includes only the uppermost 3 cm of a sapropel at its base. The reflectance records of KL17 VL and the nearby core GeoB 5844-2 [*Arz et al.*, 2003a] are congruent (Figure 3), allowing us to determine that the sapropel in KL17 VL corresponds to "*Red Sea Sapropel 1b*" in core GeoB 5844-2, dated to 10.8 ka BP [*Arz et al.*, 2003a].

4.4. Age Models

[25] The age models of the newly investigated cores KL17 VL and KL9 are based on 4 and 6 radiocarbon dates, respectively (Table 1). The calibration of radiocarbon ages from marine samples often requires large reservoir age corrections [*Casford et al.*, 2007]. This problem is accentuated in the Red Sea, where the local circulation system and the very restricted water exchange with the Indian Ocean complicate the interpretation of radiocarbon dates (see *Rohling et al.* [2008a] for details). Different rates of water exchange through Bab el Mandab, caused predominantly by changes in sea level can substantially alter the local ^{14}C reservoir correction ages. In previous studies in the Red Sea, reservoir age correction (ΔR) of between 100 and 180 years were applied [*Arz et al.*, 2003a, 2003b, 2006, 2007; *Legge et al.*, 2006, 2008]. Here, we used a ΔR of 170 years for all samples, as proposed by the *Marine Reservoir Correction Database* [*Reimer and Reimer*, 2001], with the exception of the core top in KL17 VL, where correction by more than 70 years would imply an age younger than the present-day (Table 1). In addition to uncertainty in the reservoir age, we note that radiocarbon ages based on foraminiferal calcite from Red Sea sediments may be affected by diagenetic processes [*Deuser*, 1968; *Rohling et al.*, 2008a].

[26] A correlation of cores KL17 VL and KL9 to previously investigated core KL11 [*Schmelzer*, 1998] solely on the basis of calibrated AMS radiocarbon dates would suggest that the faunal records are offset in time from one another, with an inconsistent spatiotemporal sequence through the faunal transient, which is the most striking event within these Holocene records (Figure 4). It is reasonable to assume that the faunal transient event observed across the Red Sea cores reflects the same oceanographic change that affected the entire basin, or at least a coherent/systematic sequence of changes with minor lags between the various sites. We therefore combine faunal and AMS radiocarbon data to construct an integrated age model in which the faunal transient occurs almost synchronously in all investigated cores (Figure 4).

[27] The AMS radiocarbon dates and the peak faunal transient served as tie points. These tie points were then shifted manually to achieve maximum congruency, while minimizing the resulting deviation of radiocarbon dated samples and maintaining reasonable sedimentation rates (5–10 cm/ka [*Auras-Schudnagies et al.*, 1989]). The alignment resulted in age deviation outside the 2 σ range for two radiocarbon dates (deviation from the mean calibrated ages: 519 yrs in KL9 and 221 yrs in KL17 VL) (Table 1), whereas the remaining 13 AMS radiocarbon ages could be aligned within their 2 σ calibrated age range. This approach is similar to that of *Casford et al.* [2007] in the eastern Mediterranean, where it has been shown that age uncertainties of individual AMS radiocarbon datings could amount to more than 1000 a, while the resulting mean offsets from a comprehensive age model were comparable to those found in our alignment. The resulting age model (Figure 4 and Table 1) spans 11.75 ka for KL17 VL (supported by the sapropel

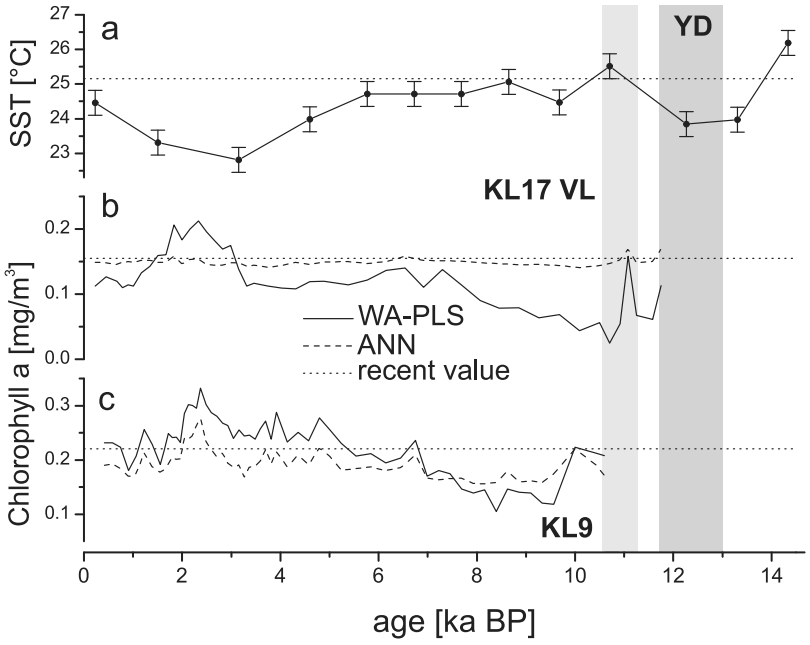

Figure 5. Temperature and productivity proxies; horizontal dotted lines mark recent proxy value at the core location. (a) Plot of TEX_{86} derived SSTs for KL17 VL based on Red Sea calibration of *Trommer et al.* [2009] (error bars: ±0.36°C), and chlorophyll *a* estimates based on planktonic foraminifera transfer functions (WA-PLS and ANN [*Siccha et al.*, 2009]) for (b) core KL17 VL and (c) core KL9. The light gray bar indicates the sapropel position and the dark gray bar the Younger Dryas [*Fairbanks*, 1990].

correlation with the well-dated core GeoB 5844-2 [*Arz et al.*, 2003a, 2003b]; Figure 3) and 10.6 ka for KL9 with the peak faunal transient around 2.4 ka BP, coinciding within age uncertainties to results of *Edelman-Furstenberg et al.* [2009]. It indicates that the tops of the records are missing, which is common with piston/gravity coring operations. One very young radiocarbon result at the top in KL17 VL might challenge our assertion based on the overall age model that the very top of the record may be missing. However, we prefer to work with a coherent 'mean' age model for the entire core section rather than to overemphasize the importance of a single dating result.

4.5. Transfer Functions

[28] Analogy of all fossil faunal assemblages to the surface data set was validated by a PCA of log-ratio transformed faunal data following the approach by *Siccha et al.* [2009]. The results indicate analog conditions between the Holocene and the core top calibration data sets, allowing us to apply the transfer functions onto all samples of both cores. Both transfer function approaches (ANN and WA-PLS) for the reconstructions of surface water productivity yield similar results for central Red Sea core KL9 (Figure 5c). Productivity shows modern values at the beginning of the record, followed by a sharp decrease after 10 ka BP and a gradual return to recent levels at around 5 ka BP. Thereafter, productivity values fluctuate around the modern level, except for a ~1.1 ka period of increased productivity between 3.1 and 2.0 ka BP.

[29] The reconstructions for northern Red Sea core KL17 VL differ considerably between the two transfer function approaches (Figure 5b). While the WA-PLS reconstructions show similar trends to the KL9 results, the ANN reconstructions in KL17 VL remain more or less constant. The lack of sensitivity of the ANN reconstructions to the dominant faunal trend seems to be caused by the low and constant abundances of *G. glutinata*. Therefore, we focus on discussing solely the WA-PLS reconstruction in KL17 VL. At the beginning of the KL17 VL record, low chlorophyll *a* values were reconstructed, increasing slowly until a plateau at 7.3 ka BP. The only excursion during the early Holocene with reconstructed productivity around recent values corresponds to the sapropel interval (Figure 5b). After 7.3 ka BP, productivity values in KL17 VL remained at around 75% of the recent level for the rest of the record, except for a period of higher productivity between 3.1 and 1.7 ka BP, similar to that in KL9. In general, the productivity reconstructions follow the patterns of relative abundance of the three main species *G. sacculifer*, *G. glutinata* and *G. ruber*. Lower productivity is reconstructed during times of dominance of *G. sacculifer* in the early Holocene and higher productivity during the faunal transient event when *G. glutinata* and *G. ruber* are more abundant.

4.6. Lipid Analyses

[30] All 13 analyzed samples contained sufficient crenarchaeotal membrane lipids to quantify GDGTs and calculate the TEX_{86} and BIT index. In the observed core section, we find BIT indices between 0.01 and 0.05 (Table 2), which are relatively low [*Hopmans et al.*, 2000] and similar to present-day average Red Sea values of 0.06 [*Trommer et al.*, 2009]. These low BIT indices indicate that there was no

Table 2. Results of the Lipid Analyses in Northern Red Sea (KL17 VL) Sediments: BIT Index, TEX_{86}, and the Derived SST (°C ± 0.36)[a]

Mean Depth (cm)	Faunal Age (ka BP)	BIT	TEX_{86}	SST (°C)
0.5	0.2	0.01	0.77	24.5
10.5	1.5	0.02	0.73	23.3
20.5	3.2	0.03	0.71	22.8
30.5	4.6	0.05	0.75	24.0
40.5	5.8	0.03	0.77	24.7
50.5	6.7	0.02	0.77	24.7
60.5	7.7	0.03	0.78	24.7
70.5	8.7	0.03	0.79	25.1
80.5	9.7	0.03	0.77	24.5
90.5	10.7	0.03	0.80	25.5
100.5	12.3	0.04	0.74	23.8
110.5	13.3	0.03	0.75	24.0
120.5	14.3	0.01	0.83	26.2

[a]Data from *Trommer et al.* [2009].

major supply of soil material by river input into the northern Red Sea during the investigated period. They also allow us to exclude the possibility of contamination of the TEX_{86} signal with soil-derived GDGTs, and we therefore interpret the TEX_{86} as pure marine temperature signal. TEX_{86} values range from 0.71 to 0.83 (Table 2). TEX_{86}-based SSTs estimates were 24°C during the Younger Dryas in the northern Red Sea and around 25°C during early Holocene (Figure 5a), which is about 1°C cooler than $U^{K'}_{37}$ temperatures of *Arz et al.* [2003a, 2003b]. The TEX_{86} temperatures then decrease to a minimum of 23°C around 3.1 ka BP, before increasing again to values corresponding to the present-day mean annual SST at the position of the core (25.2°C (M. E. Conkright et al., *World Ocean Atlas 2001*, 2001; available at http://odv.awi.de/en/data/ocean/world_ocean_atlas_2001/)).

5. Discussion

5.1. Post-Glacial Recovery of the Planktonic Ecosystem and Potential Causes of the Northern Red Sea $\delta^{18}O$ Anomaly

[31] In the northern Red Sea (KL17 VL), stable planktonic foraminifera populations start to become reestablished at about 11.7 ka BP (Figure 6a), at least 1 ka earlier than in the central Red Sea (KL9, KL11). We emphasize that this age offset is larger than the combined age uncertainties in this interval (Figures 3 and 4 and Table 1). Sea level around 12 ka BP stood about 65–70 m lower than today [*Fairbanks*, 1992; *Siddall et al.*, 2004] (Figure 6h) with estimated salinities in excess of 48 in the central Red Sea [*Almogi-Labin et al.*, 1991]. Although planktonic foraminiferal abundances of KL11 from the central Red Sea [*Schmelzer*, 1998; *Almogi-Labin et al.*, 1991] indicate that partial/intermittent recolonization of the pelagic environment occurred in this region prior to the Younger Dryas, the planktonic foraminifera abundances in both cores KL9 and KL11 (Figure 6b) show that full recovery to stable planktonic foraminifera population to average Holocene abundance levels occurred only after 10.6 ka BP, when sea level stood about 50–55 m lower than today [*Fairbanks*, 1992; *Siddall et al.*, 2004; *Biton et al.*, 2008] (Figure 6h). The central Red Sea foraminiferal faunas prior to 10.6 ka BP were dominated by high salinity tolerant species, especially during the Younger Dryas, suggesting that the habitat of the foraminifera continued to be affected by salinities close to their tolerance

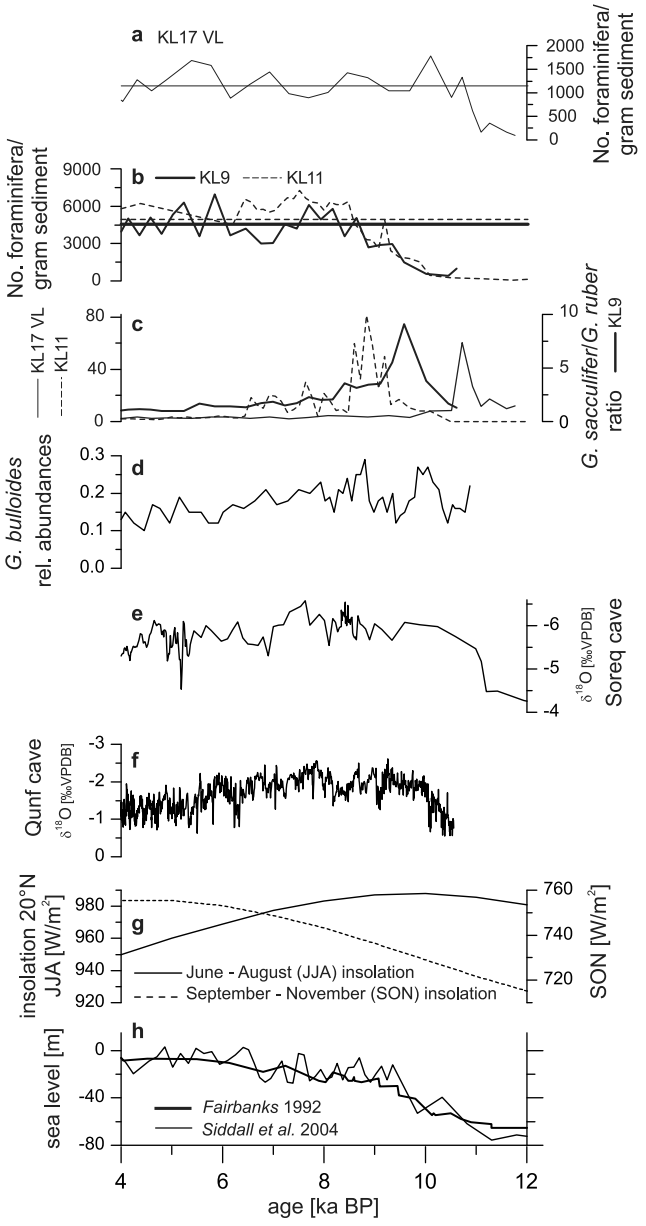

Figure 6. Graph of Red Sea faunal data and global data during the early and mid Holocene: number of foraminifera/gram sediment (a) in core KL17 VL and (b) in cores KL9 and KL11 [*Schmelzer*, 1998]; (c) *G. sacculifer*/*G. ruber* ratio of cores KL17 VL, KL11, and KL9; (d) relative abundance of *G. bulloides* in marine sediments off the coast of Oman [*Gupta et al.*, 2003]; $\delta^{18}O$ of (e) Soreq cave [*Bar-Matthews et al.*, 2003] and (f) Qunf cave [*Fleitmann et al.*, 2003] speleothems; (g) summer (JJA) and fall (SON) insolation at 20°N [W/m^2]; and (h) sea level reconstructions [*Fairbanks*, 1992; *Siddall et al.*, 2004].

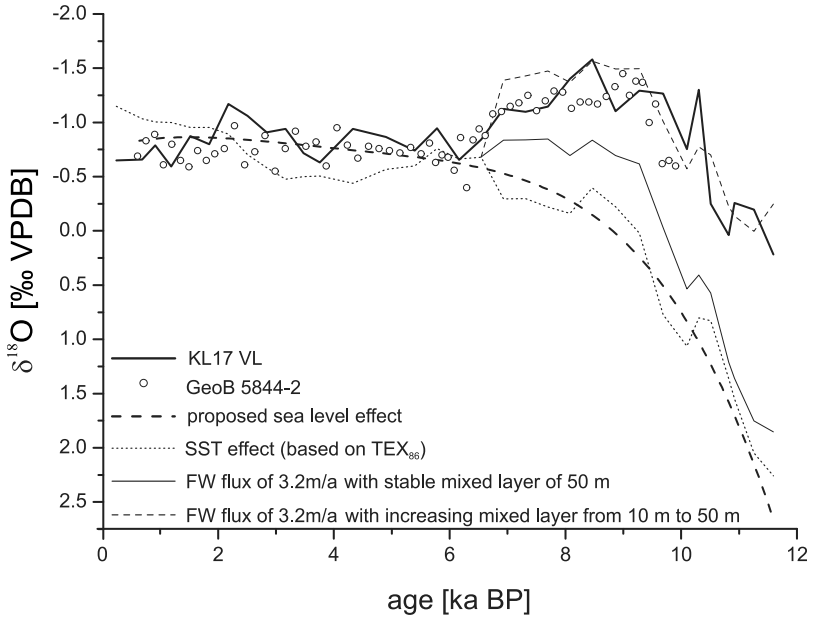

Figure 7. Observed δ^{18}O record of KL17 VL (bold solid line) (for comparison GeoB 5844-2 in dots [*Arz et al.*, 2003a]) and the proposed δ^{18}O based on sea level at 25°N in the Red Sea (bold dashed line) [*Siddall et al.*, 2004]. Calculated lines based on the proposed δ^{18}O signal show the SST effect (based on TEX_{86}) as dotted line, the freshwater (FW) flux effect of 3.2 m/a with stable mixed layer depth (50 m) as thin solid line, and the FW flux effect of 3.2 m/a with increasing mixed layer from 10 m at 11.7 ka BP to 50 m at 6.5 ka BP as thin dashed line. Increased FW flux and mixed layer influence is considered for instantaneous mixing and only until 6.5 ka BP, since when the observed and proposed δ^{18}O signals are coinciding.

limit. The low abundance values of these early faunas suggest that the earliest colonization of the central Red Sea was discontinuous, with intermittent development of foraminiferal assemblages in temporarily established (critical) habitats. In the northern Red Sea fauna, no significant traces of the earliest recolonization(s) are observed, but faunas reappear by about 11.7 ka BP and then recover sharply to average Holocene abundance levels as early as 10.5 ka BP, characterized by typical Holocene assemblages dominated by *G. sacculifer*.

[32] Given that salinity in the Red Sea increases strongly with lowering of sea level [*Rohling et al.*, 1998; *Siddall et al.*, 2003, 2004] and with evaporation in the north, the basin salinity should have been much higher during the planktonic foraminiferal recolonization in the north than in the central Red Sea. Yet, total numbers of foraminifera in northern core KL 17 VL show that by 11.7 ka BP, surface water salinity in northern Red Sea must have decreased to lower than 47 (critical salinity for survival of *G. sacculifer* [*Hemleben et al.*, 1989]), making it possible for foraminifera to reach average Holocene population levels at around 10.5 ka BP, whereas in the central Red Sea, average Holocene population levels were reached only after 9 ka BP (Figure 6b). The increase in foraminiferal abundance in KL17 VL coincides with a steep decrease in δ^{18}O between 11.7 and 10.3 ka BP (Figure 3), which suggests that the re-colonization in the northern Red Sea was associated with a rapid change in water chemistry. According to *Fairbanks* [1992], *Bard et al.* [1990], *Fairbanks* [1990] and *Siddall et al.* [2004], sea level at the time of the isotopic shift between 11.7 and 10.3 ka BP in KL17 VL rose by about 15–20 m, translating into a δ^{18}O shift of ~ −0.6 to −1.0‰ (19°N/25°N curve in the work by *Siddall et al.* [2004] (Figure 7) or −0.7‰ according to *Arz et al.* [2007]). While the magnitude of the δ^{18}O shift is consistent with the maximum expected change in the seawater isotopic composition (~−1.0‰) due to the rising sea level at that time, the absolute values of δ^{18}O are offset from the expected values by more than 1‰ until 6 ka (more than 2‰ in the earliest Holocene; Figure 7).

[33] The sea surface warming suggested by TEX_{86} at the beginning of our record amounted to about 1°C (Figure 5), which could explain an additional shift in δ^{18}O of *G. ruber* of up to −0.25‰ (Figure 7). This leaves up to 1.75‰ of the observed offset to be explained. This isotopic shift is significantly larger than that invoked by *Arz et al.* [2003a], who attempted to explain only the 0.5‰ difference between the early and later Holocene values, not accounting for changes in stable isotopic composition of basin seawater due to the rising sea level.

[34] *Arz et al.* [2003a] suggested that their inferred additional moisture source from the north became important from around 9.75 ka BP. However, when the full offset from the expected sea level driven isotope curve is considered (Figure 7), the onset of such an excess freshwater flux into the northern Red Sea appears to have occurred around 1300 years earlier, at around the end of the Younger Dryas.

This would be consistent with data from Soreq cave, Israel, which has been interpreted in terms of enhanced precipitation from 11 ka BP [*Bar-Matthews et al.*, 1999] (Figure 6e). Although our earlier date for the onset of the additional (Mediterranean) moisture influence relies on one single radiocarbon date in core KL17 VL, the 1.3 ka difference with the suggested date of *Arz et al.* [2003a] is significantly larger than the combined chronological uncertainties. The good correlation of the $\delta^{18}O$ values and the "*Red Sea Sapropel 1b*" of KL17 VL with those in the well-dated core GeoB 5844-2 [*Arz et al.*, 2003a, 2003b] (Figure 3) supports our age model for KL17 VL.

[35] To investigate what hydrological factors are required to cause this shift in $\delta^{18}O$ we consider several alternative volumetric calculations. Assuming an annual mixed layer thickness of 50 m with the observed $\delta^{18}O$ of 0‰ (at 11.5 ka BP) and a net evaporation $\delta^{18}O$ of at least −8‰ [*Herold and Lohmann*, 2009], a precipitation-induced $\delta^{18}O$ anomaly of −1.75‰, would amount to extreme values in excess of 2 m/a precipitation over the Gulf of Aqaba and the adjoining catchment area (minimum estimate of appr. 40 km around the coastline) [((50m * $0‰_{water}$ − (−1.75‰$_{precip}$) * 50m)/(0‰ − (−8‰$_{net\ evap}$))*3600 $km^2_{GOA\ surface\ area\ (north\ of\ 28\ °N)}$)/18000 $km^2_{GOA\ plus\ catchment\ area}$]. For what is currently one of the driest places on earth these values are certainly out of range, although enhanced runoff into the Gulf of Aqaba and the northern Red Sea has been previously suggested to be responsible for lowered salinities in this region after the deglaciation [*Winter*, 1982; *Locke and Thunell*, 1988; *Naqvi and Fairbanks*, 1996; *Arz et al.*, 2003a], and although active Wadis in Jordan were recorded for that time [*Niemi et al.*, 2001]. Even a precipitation-induced $\delta^{18}O$ anomaly of only −0.5‰, as proposed by *Arz et al.* [2003a], would require over 0.62 m/a precipitation over the region [(50m * $0‰_{water}$ − (−0.5‰$_{precip}$) * 50m)/(0‰ − (−8‰$_{net\ evap}$))*3600 $km^2_{GOA\ surface\ area\ (north\ of\ 28\ °N)}$)/18000 $km^2_{GOA\ plus\ catchment\ area}$], which means an excess freshwater flux into the northern Red Sea equivalent to 3.2 m/a, reducing salinity by from 50 to 47 and leaving −1.25‰ of the observed offset still to be explained. The required precipitation is difficult to reconcile with precipitation estimates from speleothems in Israel, which imply a maximum value in the early Holocene of 1 m/a in Soreq cave, with a strong decrease toward the south [*Bar-Matthews et al.*, 1999, 2000, 2003]. Even some of our own data fail to support the idea of a precipitation/runoff event, given that the BIT indices (Table 1) suggest the absence of any major supply of soil material by river input.

[36] The above calculations are based on instantaneous mixture and constant surface water turnover in the northern Red Sea. In the presence of a strong stratification, the observed oxygen isotope anomaly could have accumulated in a time-transient manner over many years, requiring a much smaller change in the annual hydrological balance. Indeed, the existence of the sapropel in KL17 VL (supported by XRF data [*Trommer*, 2009]) and benthic foraminifera assemblages in the northern Red Sea [*Badawi*, 2003] indicate dysoxic conditions on the seafloor at the beginning of the isotopic anomaly, pointing toward a triggering of the anomaly during times of sea level rise and strong stratification of the water column [*Arz et al.*, 2003b; *Almogi-Labin et al.*, 1991]. Under such conditions, a freshwater excess, of only 0.4 m/a (translated into a precipitation of 0.08 m/a over the catchment region and draining entirely into the northern Red Sea) would have been sufficient to build up an −1.75 ‰ anomaly in about 260 years. However, it will at the same time reduce the salinity in the mixed layer below 10, making it uninhabitable for planktonic foraminifera. This simple box-model calculation considers an evaporation rate of 2 m/a ($\delta^{18}O_{evap}$ = −8‰, $\delta^{18}O_{precip}$ = −7‰ [*Herold and Lohmann*, 2009]) and a constant mixed layer depth of 50m, with the freshwater excess being compensated by convective/lateral loss. Importantly, the salinity decline associated with the isotopic shifts remains the same independent of the amount of excess freshwater flux (which only influences the time necessary to build up the anomaly). Therefore, it seems unlikely that the oxygen isotopic anomaly could have been built during a time-transient process without significant changes in some other variable.

[37] One other variable that significantly affects the inferred amount of excess precipitation is the thickness of the mixed-layer habitat occupied by *G. ruber*. However, during the progression of the oxygen anomaly, there are no indications of a continued strong stratification of the water column throughout the year as pteropods and benthic foraminifera reflect well oxygenated intermediate and bottom waters [*Almogi-Labin et al.*, 1991; *Badawi*, 2003; *Geiselhart*, 1998]. Therefore, although the observed isotopic anomaly may have originated in incremental time-transient processes, it could not have been maintained under such conditions throughout its observed duration. Once deep water formation resumed in the northern Red Sea, the stratification would have been disrupted and the isotopic anomaly would have to be constantly renewed, as assumed in the instantaneous mixture model. As the results of the instantaneous mixture model appear unrealistic and a transient scenario can only potentially explain the onset of the anomaly, we explore other possible changes in the Red Sea hydrography to explain the observed $\delta^{18}O$ offset and to identify likely contributing processes and their relative importance.

[38] Considering changes in the mixed layer depth for an instantaneous mixing scenario, the $\delta^{18}O$ shift could be explained by a change in mixed-layer thickness from 10 m at the beginning of our record to 50 m at 6.5 ka BP (Figure 7) at a freshwater flux of 3.2 m/a, throughout the early Holocene humid period in the northern Red Sea (11.7–6.5 ka BP). Since there is no analog to such mixed-layer depth at present, it must remain a speculation whether a) such freshwater lenses would present a sufficiently large habitat for planktonic foraminifera, and/or b) it would be possible to maintain a 10-m mixed layer in the presence of intense year-round northerly winds in the region [*Pedgley*, 1974]. Even if anomalous mixed-layer conditions were involved, we infer that it is highly unlikely that the entire magnitude of the observed isotopic offset could be uniquely explained in terms of freshwater forcing.

[39] The early onset of the isotopic offset, and the unrealistically high implied precipitation increase over the region, call for alternative explanations or additional processes affecting the surface water isotopic composition

during the humid period. Processes that could contribute toward lighter isotopic composition in the northern Red Sea include substantially reduced evaporation and/or weaker isotopic fractionation upon evaporation [*Rohling*, 1999]. Both of these processes would imply increased relative humidity. Reduced evaporation alone cannot account for the observed pattern, because the surface water in the central Red Sea in the earliest Holocene (KL9; Figure 3 [see also *Arz et al.*, 2003a]) was isotopically similar to that in the northern Red Sea, but with salinity above 47, as evidenced by the reduced occurrence of planktonic foraminifera, until 10.6 ka BP (except between 13.2 and 12.4 ka BP in KL11 [*Schmelzer*, 1998]). The northern Red Sea surface water thus could not have derived from the central Red Sea without an addition of excess freshwater. Even a drastic reduction in evaporation rate alone from the present-day value of 2 m/a to lower than 0.5 m/a could account for only 0.1–0.4‰ of the isotopic offset (assuming δ^{18}O of evaporating vapor of −8‰ and δ^{18}O of seawater between 0 and −2‰). The only possibility to explain the remaining 1.25‰ of the isotopic offset (by taking the minimum excess freshwater flux of 3.2 m/a), would require an increase in relative humidity from 0.6 to 0.8 at atmospheric δ^{18}O of −16‰ [*Rohling*, 1999]. Therefore, we suggest that only an additional increase of relative air humidity with evaporation fractionation could account for the large observed δ^{18}O offset between about 12 and about 6 ka BP (Figure 7) in the northern Red Sea region and none of the other considered processes by itself are likely to account for the observed magnitude of isotopic offset. The inferred increased relative humidity may have been related to the concomitant general monsoon maximum and the circum-Mediterranean moisture maximum at that time [e.g., *Rohling*, 1999].

5.2. Early Holocene Insolation Trend

[40] Faunal records throughout the Red Sea (Figures 4 and 6c) [*Schmelzer*, 1998] indicate that following the initial recovery of the planktonic ecosystem, a foraminiferal fauna was established that was characterized by high abundances of *G. sacculifer*. This fauna indicates that the salinity in the surface layer decreased below the tolerance maximum of all foraminifera species. *G. sacculifer* reaches highest abundances at the beginning of this phase and declines in the subsequent 3.5 ka (KL17 VL) and 4.5 ka (KL9) (Figure 6c). Since the Red Sea circulation system is determined by seasonally changing monsoon winds, the gradual decline of *G. sacculifer* likely represents a gradual change in the circulation of the basin controlled by the monsoon winds, following the summer insolation decline (Figure 6g). This agrees with observations in the Arabian Sea, where *Gupta et al.* [2003] found that *G. bulloides* abundances (Figure 6d) were high during the early Holocene and then steadily declined with decreasing monsoon intensity due to declining Holocene summer insolation (this monsoon trend was also highlighted by *Overpeck et al.* [1996] and *Fleitmann et al.* [2003, 2007]).

[41] Although *G. bulloides* records in the Arabian Sea indicate increased upwelling of nutrient-rich waters due to strong SW Monsoons in the early Holocene [*Gupta et al.*, 2003], the high abundance of *G. sacculifer* in the Red Sea is more consistent with oligotrophic conditions [*Siccha et al.*, 2009]. This seems counterintuitive: if the waters entering the Red Sea from the south during the SW Monsoon were more nutrient rich due to more intense upwelling, then one might expect a higher productivity within the Red Sea as well. The explanation lies in the spatial expression of the monsoon circulation within the Red Sea and its impact on productivity. Today, enhanced productivity is indeed observed during the summer months (June–September) in the Red Sea when the SW Monsoon occurs, but it is always limited to the very south of the basin, following the extent of the intermediate layer of nutrient-rich water that enters the basin from the Gulf of Aden (G. C. Feldman and C. R. McClain, online data, 2006). In contrast, the central and northern sectors of the Red Sea remain less productive during the summer season [*Weikert*, 1987; *Veldhuis et al.*, 1997; G. C. Feldman and C. R. McClain, online data, 2006]. Therefore, times of stronger/longer summer monsoons, determining longer summer circulation conditions in the Red Sea, would cause low nutrient availability (average annual mean) in the central and northern Red Sea, where nutrient availability is linked to winter convective mixing. This scenario is consistent with the dominance of *G. sacculifer* in our records and the related low productivity reconstruction (Figures 5b and 5c). It also explains the observed trends in foraminiferal stable carbon isotopes (Figure 2) and in sedimentary nitrogen isotopes (Figure 2b), which are more negative and so suggest reduced productivity in the early Holocene, followed by a trend to heavier values that suggest increasing productivity. These trends are in good agreement with the *G. sacculifer* decline and the reconstructed productivity increase from the central to northern Red Sea, further supporting our hypothesis of a gradual circulation-change-induced increase in productivity through the Holocene in the Red Sea, as the SW monsoon progressively weakened and winter processes gained in relative importance.

[42] The consistent influence of the early Holocene insolation trend on the Red Sea circulation, as shown by planktonic foraminiferal faunas and sediment properties in our records, ended at approximately 7.3 ka BP in KL17 VL and 5.1 ka BP in KL9 (Figure 6c). The difference in timing between the two sites is beyond the age model uncertainties and suggests a meridionally progressive weakening of the Indian SW Monsoon influence. This is particularly clear from the earlier termination of the *G. sacculifer* decline in the northern Red Sea (7 ka BP) than in the central Red Sea (5 ka BP), followed by the end of the *G. bulloides* decline of the coast of Oman at around 1.8 ka BP [*Gupta et al.*, 2003]. Similar meridional asynchroneity was observed by *Fleitmann et al.* [2007] in speleothem precipitation records from Oman and Socotra during the mid Holocene. *Fleitmann et al.* [2007] interpreted the trend they observed as a result of a gradual southward withdrawal of the maximum northward penetration of the summer ITCZ.

5.3. Millennial-Scale Variability

[43] Our faunal records reveal the presence of only one distinct millennial-scale event within the Holocene, the 'faunal transient' between 3.1 to 1.7 ka BP (Figure 8).

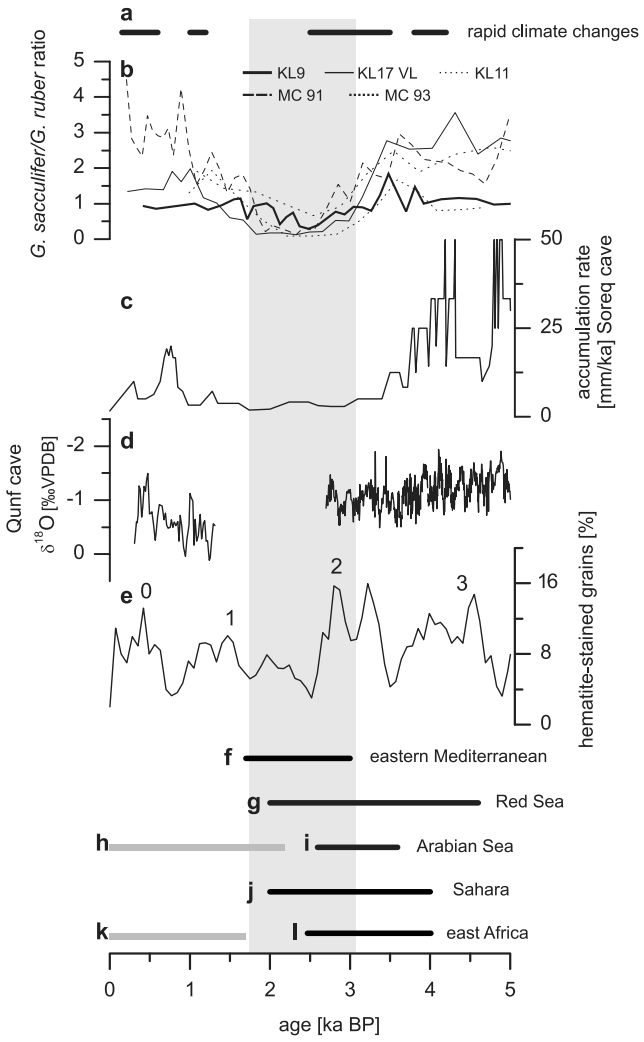

Figure 8. Graph of Red Sea faunal data and global data during the mid and late Holocene: (a) rapid climate change events after *Mayewski et al.* [2004]; (b) G. sacculifer/G. ruber ratio of cores KL17 VL, KL9, KL11 [*Schmelzer*, 1998], MC93, and MC91 [*Edelman-Furstenberg et al.*, 2009]; (c) accumulation rate [mm/ka] of speleothem rings in Soreq cave [*Bar-Matthews et al.*, 2003]; (d) $\delta^{18}O$ of Qunf cave speleothem [*Fleitmann et al.*, 2003]; (e) hematite-stained grains [%] of North Atlantic sediments (numbers indicate Bond events 0 - 3) [*Bond et al.*, 2001]; interval of recorded dry periods (black bars) in (f) the eastern Mediterranean [*Schilman et al.*, 2001], (g) the Red Sea [*Almogi-Labin et al.*, 1991], (i) the Arabian Sea [*Caratini et al.*, 1994; *Doose-Rolinski et al.*, 2001], (j) the Sahara [*Petite-Maire et al.*, 1997], and (l) east Africa [*Gasse and Van Campo*, 1994]; and interval of recorded moist periods (horizontal dark gray bars) (h) in the Arabian Sea [*Caratini et al.*, 1994] and (k) in east Africa [*Mawson and Williams*, 1984]. Light gray bar indicates pronounced winter circulation mode recorded in Red Sea sediments.

Within the uncertainties of its age constraints in our records (Figure 4), the timing of this event, which is starting to develop at 3.6 ka BP, corresponds to that of a millennial event in the North Atlantic [*Bond et al.*, 1997]. This Bond event 2 has also been recognized in the Aegean Sea [*Casford et al.*, 2001; *Rohling et al.*, 2002; *Ehrmann et al.*, 2007] and in the Arabian Sea [*Berger and von Rad*, 2002] and indeed may have a very wide distribution [*Mayewski et al.*, 2004]. In our central and northern Red Sea records, this event is characterized by high abundances of *G. ruber* (as also observed from *Badawi* [1997], *Schmelzer* [1998] and *Edelman* [1996]). A combination of our data with records from three other radiocarbon-dated central Red Sea cores (KL11 [*Schmelzer*, 1998] and multi cores MC93 and MC91 [*Edelman-Furstenberg et al.*, 2009]; Figure 1) highlights the ubiquitous nature of this event throughout the central and northern Red Sea (Figure 8b). Faunas with high *G. ruber* abundances are today limited to the central to southern Red Sea [*Siccha et al.*, 2009] and we interpret them as a manifestation of relatively enhanced productivity in the foraminiferal habitat within the basin. The faunal transient suggests that this enhanced surface productivity extended to the northern Red Sea. This is corroborated by our transfer-function based productivity reconstruction (Figures 5b and 5c), by slightly enhanced $\delta^{13}C$ values in KL17 VL (Figure 2a), and slightly enhanced nitrogen isotope values in KL9 (Figure 2b).

[44] As discussed above, the summer circulation mode in the Red Sea entails reduced nutrient availability in the central Red Sea. Dominance of *G. ruber* throughout the Red Sea during the faunal transient would imply that the circulation changed toward a situation with more dominant winter-type conditions that led to more productive surface waters. Cooler/more intense winter conditions in the northern Red Sea during the time of the faunal transient are supported by our temperature reconstructions from core KL17 VL (Figure 5a), and are consistent with data from a wide region across east Africa [*Bonnefille et al.*, 1990; *Thompson et al.*, 2002] and the eastern Mediterranean Sea [*Emeis et al.*, 2000; *Rohling et al.*, 2002] (see also summary in the work by *Rimbu et al.* [2004]). Enhanced intensity/duration of winter-type conditions over the Red Sea, as suggested by our data, would agree with a monsoon trend in the Arabian Sea between 3.5 and 2.0 ka BP that was opposite to the monsoon trend from 10 to 6 ka BP [*Sarkar et al.*, 2000]. Similarly, records throughout the Arabian Sea suggest an intensification of the winter monsoons during that time [*Doose-Rolinski et al.*, 2001; *Lückge et al.*, 2001; *von Rad et al.*, 2006] (Figure 1a), as well as a minimum for Holocene SW (summer) Indian Monsoon strength around 3.5 ka BP [*Naidu and Malmgren*, 1996; *Phadtare*, 2000]. The interval 4–2 (3.5–2.5) ka BP appears to be characterized by a significant aridification throughout the region [*Mayewski et al.*, 2004], with clear manifestations in terrestrial climate records from the Middle East region [*Bar-Matthews et al.*, 1999; *Fleitmann et al.*, 2003] and northern Africa [*Gasse and Van Campo*, 1994; *Petite-Maire et al.*, 1997] (Figure 8).

[45] Today, wind stress over the Red Sea is higher in winter than in summer [*Sofianos and Johns*, 2001], causing

higher evaporation rates [*da Silva et al.*, 1994] and increased rates of deep-water formation [*Sofianos and Johns*, 2003]. Higher abundances of the mesopelagic pteropod *Limacina bulimoides* from the Red Sea have been used to suggest improved oxygenation of intermediate waters between 4.6 and 2 ka BP, which may reflect generally increased deep-water ventilation at that time [*Almogi-Labin et al.*, 1991; *Edelman-Furstenberg et al.*, 2009] (Figure 8g). Our inferred cause for the faunal transient in terms of an increase in winter intensity over the northern Red Sea is in good agreement with the prevalence of more intense winter conditions (with frequent northerly outbreaks of cold polar/continental air) over the northern sectors of the eastern Mediterranean [*Rohling et al.*, 2002]. We speculate that the winter-time outbreaks of cool air masses, as documented over the eastern Mediterranean, may have extended into the northern Red Sea region, causing more intense winter-type circulation conditions and thus leading to the development of the faunal transient.

[46] By analogy to modern conditions in winter, we infer that intensified winter-type conditions would likely be associated with enhanced surface water advection from more southern sites toward the northern Red Sea. The 0.3‰ excursion of *G. ruber* δ^{18}O in KL17 VL toward lighter values during the faunal transient (Figure 2) may have resulted from such enhanced advection of surface waters from the south.

[47] The combination of micropaleontological and geochemical analyses of marine sediment cores from the Red Sea allowed us to identify the interplay between impacts from the Mediterranean climate and the Indian Monsoon in this region. Yet, despite the strong manifestation of the event around 3.1 - 1.7 ka BP, other well-known and distinct Holocene climate events like the 8.2 and 4.2 ka BP droughts [*Barber et al.*, 1999; *Staubwasser et al.*, 2003] are not recognized in our records. The lack of the 4.2 ka BP event could possibly be attributed to the relatively low resolution of the studied sediment cores compared to the laminated sediment cores in the Red Sea [*Seeberg-Elverfeldt et al.*, 2005; *Arz et al.*, 2006; *Lamy et al.*, 2006], where a higher temporal resolution could be achieved and where a manifestation of the 4.2 ka BP could be found [*Arz et al.*, 2006; *Edelman-Furstenberg et al.*, 2009]. On the other hand, the 4.2 ka BP event is not recorded in the majority of the available Arabian Sea records. There is evidence that this short-term event [*Staubwasser et al.*, 2003] was recorded mainly in terrestrial or terrestrial-influenced settings [*Marchant and Hooghiemstra*, 2004] and that the atmospheric fluctuations potentially responsible for this event had a more pronounced effect on temperate latitudes [*Marchant and Hooghiemstra*, 2004; *Staubwasser and Weiss*, 2006], which could be a further the reason why the event is so inconsistently recorded in the (sub-) tropical Red Sea and Arabian Sea.

[48] The lack of the 8.2 ka BP event in our records is in agreement with other Red Sea climate records [*Almogi-Labin et al.*, 1991; *Arz et al.*, 2003a; *Geiselhart*, 1998; *Schmelzer*, 1998; *Siddall et al.*, 2003], which suggests that the centennial-scale weakening of the Indian SW Monsoon from 8.5 to 8.0 ka BP [*Rohling and Pälike*, 2005; *Cheng et al.*, 2009] did not cause sufficiently pervasive changes in the Red Sea to be apparent in the planktonic foraminiferal data.

5.4. Establishment of the Modern Circulation Pattern in the Red Sea

[49] All investigated proxies show that modern circulation conditions became established in the Red Sea upon termination of the faunal transient, by 1.7 ka BP. The last two millennia (excluding the last ~300 years which were not recovered) appear to have been characterized by conditions without extreme aridity or intense (cooler and more arid) winter conditions. The reestablishment of fluvial depositions in the Red Sea hills of Sudan [*Mawson and Williams*, 1984], the resumption of flow-stone deposition on the Arabian Peninsula [*Fleitmann et al.*, 2003] and pollen data from the Arabian Sea [*Caratini et al.*, 1994] all bear witness to the return of relatively more humid conditions to the region (Figure 8). Other marine records from the Red Sea [*Almogi-Labin et al.*, 1991] and the Mediterranean Sea [*Schilman et al.*, 2001] also indicate the establishment of modern circulation patterns between 1.7 and 2 ka BP.

6. Conclusions

[50] New multiproxy paleoceanographic data have been generated for two sediment cores from the Red Sea in order to investigate millennial-scale climate fluctuations in this region during the Holocene and to examine the influence of insolation forced climate systems like the Indian Monsoon on the Red Sea's circulation dynamics. In the early Holocene, light δ^{18}O values and high abundances of planktonic foraminifera in the northern Red Sea suggest lower salinities than what would be expected from the postglacial sea level rise alone. These observations are consistent with the existence of higher relative air humidity [*Rohling*, 1999], reduced isotopic fractionation upon evaporation and enhanced freshwater flux, and we show that these processes have affected the northern Red Sea as early as by 11 ka BP, simultaneously with the increase in precipitation recorded in stalagmites in Israel [*Bar-Matthews et al.*, 1999].

[51] The early Holocene conditions in the Red Sea are largely recording the insolation-forced gradual decline in the strength of the Indian SW Monsoon, which causes low productivity in the central and northern Red Sea due to extended summer circulation conditions. The final decline of the Indian SW Monsoon is diachronous in the Red Sea, occurring earlier in the northern Red Sea than in the central Red Sea. A pronounced millennial-scale event is manifested in the faunal records between 3.1 and 1.7 ka BP, which may be caused by more intensified winter-type conditions (possibly referring to an enhanced winter (NE) Monsoon) with cool air masses coming over the Red Sea from the Mediterranean Sea. Enhanced evaporation in the north thus favors the winter circulation mode and associated higher productivity in the Red Sea. Modern climate and circulation conditions have been established after 1.7 ka BP. Our results emphasize that at times of sea level highstands the Red Sea is sensitive to insolation-driven processes and their effects on the intensity, spatial extent and seasonal pattern of regional climate systems.

[52] **Acknowledgments.** This project was supported by Deutsche Forschungsgemeinschaft (DFG KU 2259/3-1 "RedSTAR," He 697/16-18). We are grateful to Hartmut Schulz for constructive and fruitful discussions. We thank Editor Gerald Dickens, two anonymous referees, and Mark Siddall for constructive comments which helped to improve this manuscript. We would like to thank Valentina Cruz, Sofie Jehle, and Alexander Floria (all University of Tübingen) for micropaleontological sample preparation. This study contributes to UK NERC projects NA/C003152/1 and NE/E01531X/1. M.v.d.M. and S.S. were funded by the European Science Foundation (ESF) under the EUROCORES Program "EuroCLIMATE," through contract ERAS-CT-2003-980409 of the European Commission, DG Research, FP6 and by the Dutch Organization for Scientific Research (NWO), Earth and Life Sciences (ALW), through grant 818.07.022 and a VICI grant to S.S. NWO is also acknowledged for supporting the Dutch part of the ESF program. Anchelique Mets, Ellen Hopmans, and Michiel Kienhuis (NIOZ) are thanked for help with the organic geochemical measurements. We are thankful to crew and cruise leader of RV Meteor 5/2 and 31/2.

References

Alley, R. B., P. A. Mayewski, T. Sowers, M. Stuiver, K. C. Taylor, and P. U. Clark (1997), Holocene climatic instability: A prominent widespread event 8200 years ago, *Geology*, *25*, 483–486, doi:10.1130/0091-7613(1997)025<0483:HCIAPW>2.3.CO;2.

Almogi-Labin, A. (1982), Stratigraphic and paleoceanographic significance of late Quaternary pteropods from deep-sea cores in the Gulf of Aqaba (Elat) and northernmost Red Sea, *Mar. Micropaleontol.*, *7*, 53–72, doi:10.1016/0377-8398(82)90015-9.

Almogi-Labin, A., C. Hemleben, D. Meischner, and H. Erlenkeuser (1991), Paleoenvironmental events during the last 13,000 years in the central Red Sea as recorded by pteropoda, *Paleoceanography*, *6*, 83–98, doi:10.1029/90PA01881.

Almogi-Labin, A., C. Hemleben, and D. Meischner (1998), Carbonate preservation and climatic changes in the central Red Sea during the last 380 kyr as recorded by pteropods, *Mar. Micropaleontol.*, *33*, 87–107, doi:10.1016/S0377-8398(97)00034-0.

Almogi-Labin, A., M. Bar-Matthews, and A. Ayalon (2004), Climate variability in the Levant and northeast Africa during the Late Quaternary based on marine and land records, in *Human Paleoecology in the Levantine Corridor*, edited by N. Goren-Inbar and J. D. Speth, pp. 117–134, Oxbow, Oxford, U. K.

Arz, H. W., F. Lamy, J. Pätzold, P. J. Müller, and M. Prins (2003a), Mediterranean moisture source for an Early Holocene humid period in the northern Red Sea, *Science*, *300*, 118–121, doi:10.1126/science.1080325.

Arz, H. W., J. Pätzold, P. J. Müller, and M. O. Moammar (2003b), Influence of Northern Hemisphere climate and global sea level rise on the restricted Red Sea marine environment during termination I, *Paleoceanography*, *18* (2), 1053, doi:10.1029/2002PA000864.

Arz, H. W., F. Lamy, and J. Pätzold (2006), A pronounced dry event recorded around 4.2 ka in brine sediments from the northern Red Sea, *Quat. Res.*, *66*, 432–441, doi:10.1016/j.yqres.2006.05.006.

Arz, H. W., F. Lamy, A. Ganopolski, N. Nowaczyk, and J. Pätzold (2007), Dominant Northern Hemisphere climate control over millennial-scale glacial sea-level variability, *Quat. Sci. Rev.*, *26*, 312–321, doi:10.1016/j.quascirev.2006.07.016.

Auras-Schudnagies, A., D. Kroon, G. Ganssen, C. Hemleben, and J. E. Van Hinte (1989), Distributional pattern of planktonic foraminifers and pteropods in surface waters and top core sediments of the Red Sea, and adjacent areas controlled by the monsoonal regime and other ecological factors, *Deep Sea Res., Part A*, *36*, 1515–1533, doi:10.1016/0198-0149(89)90055-1.

Badawi, A. (1997), Planktonic foraminifera as paleoecological indicators in the northern Red Sea, M.Sc. thesis, 81 pp., Alexandria Univ., Alexandria, Egypt.

Badawi, A. (2003), Reconstruction of Late Quaternary paleoceanography of the Red Sea: Evidence from benthic foraminifera, *Tueb. Mikropaläontol. Mitt.*, *28*, 1–87.

Barber, D. C., et al. (1999), Forcing of the cold event of 8,200 years ago by catastrophic drainage of Laurentide lakes, *Nature*, *400*, 344–348, doi:10.1038/22504.

Bard, E., B. Hamelin, R. G. Fairbanks, and A. Zindler (1990), Calibration of the ^{14}C timescale over the past 30,000 years using mass spectrometric U-Th ages from Barbados corals, *Nature*, *345*, 405–410, doi:10.1038/345405a0.

Bar-Matthews, M., A. Ayalon, A. Kaufman, and G. J. Wasserburg (1999), The eastern Mediterranean paleoclimate as a reflection of regional events: Soreq cave, Israel, *Earth Planet. Sci. Lett.*, *166*, 85–95, doi:10.1016/S0012-821X(98)00275-1.

Bar-Matthews, M., A. Ayalon, and A. Kaufman (2000), Timing and hydrological conditions of sapropel events in the eastern Mediterranean, as evident from speleothems, Soreq cave, Israel, *Chem. Geol.*, *169*, 145–156, doi:10.1016/S0009-2541(99)00232-6.

Bar-Matthews, M., A. Ayalon, M. Gilmour, A. Matthews, and C. J. Hawkesworth (2003), Sea-land oxygen isotopic relationships from planktonic foraminifera and speleothems in the eastern Mediterranean region and their implication for paleorainfall during interglacial intervals, *Geochim. Cosmochim. Acta*, *67*, 3181–3199, doi:10.1016/S0016-7037(02)01031-1.

Berger, W. H., and U. von Rad (2002), Decadal to millennial cyclicity in varves and turbidites from the Arabian Sea: Hypothesis of tidal origin, *Global Planet. Change*, *34*, 313–325, doi:10.1016/S0921-8181(02)00122-4.

Berggren, W. A., and A. Boersma (1969), Late Pleistocene and Holocene planktonic foraminifera from the Red Sea, in *Hot Brines and Recent Heavy Metal Deposits in the Red Sea*, edited by E. T. Degens and D. A. Ross, pp. 282–298, Springer, Berlin.

Bianchi, G. G., and I. N. McCave (1999), Holocene periodicity in North Atlantic climate and deep-ocean flow south of Iceland, *Nature*, *397*, 515–517, doi:10.1038/17362.

Biton, E. (2006), The Red Sea during the Last Glacial Maximum, M.S. thesis, 93 pp., Weizmann Inst. of Sci., Rehovot, Israel.

Biton, E., H. Gildor, and W. R. Peltier (2008), Red Sea during the Last Glacial Maximum: Implications for sea level reconstruction, *Paleoceanography*, *23*, PA1214, doi:10.1029/2007PA001431.

Bond, G., et al. (1997), A pervasive millennial-scale cycle in North Atlantic Holocene and glacial climates, *Science*, *278*, 1257–1266, doi:10.1126/science.278.5341.1257.

Bond, G., et al. (2001), Persistent solar influence on North Atlantic climate during the Holocene, *Science*, *294*, 2130–2136, doi:10.1126/science.1065680.

Bonnefille, R., J. C. Roeland, and J. Guiot (1990), Temperature and rainfall estimates for the past 40,000 years in equatorial Africa, *Nature*, *346*, 347–349, doi:10.1038/346347a0.

Brachert, T. C. (1999), Non-skeletal carbonate production and stromatolite growth within a Pleistocene deep ocean (Last Glacial Maximum, Red Sea), *Facies*, *40*, 211–228, doi:10.1007/BF02537475.

Caratini, C., I. Bentaleb, M. Fontugne, M. T. Morzadec-Kerfourn, J. P. Pascal, and C. Tissot (1994), A less humid climate since ca. 3500 yr B.P. from marine cores off Karwar, western India, *Palaeogeogr. Palaeoclimatol. Palaeoecol.*, *109*, 371–384, doi:10.1016/0031-0182(94)90186-4.

Casford, J. S. L., et al. (2001), Mediterranean climate variability during the Holocene, *Mediterr. Mar. Sci.*, *2*(1), 45–55.

Casford, J. S. L., R. Abu-Zied, E. J. Rohling, S. Cooke, C. Fontanier, M. Leng, A. Millard, and J. Thomson (2007), A stratigraphically controlled multiproxy chronostratigraphy for the eastern Mediterranean, *Paleoceanography*, *22*, PA4215, doi:10.1029/2007PA001422.

Cember, R. P. (1988), On the sources, formation, and circulation of Red Sea Deep Water, *J. Geophys. Res.*, *93*, 8175–8191, doi:10.1029/JC093iC07p08175.

Cheng, H., et al. (2009), Timing and structure of the 8.2 kyr B.P. event inferred from $\delta^{18}O$ records of stalagmites from China, Oman, and Brazil, *Geology*, *37*, 1007–1010, doi:10.1130/G30126A.1.

Clifford, M., C. Horton, J. Schmitz, and L. H. Kantha (1997), An oceanographic nowcast/forecast system for the Red Sea, *J. Geophys. Res.*, *102*, 25,101–25,122.

Cullen, M., P. B. deMenocal, S. Hemming, G. Hemming, F. H. Brown, F. H. Guilderson, and F. Sirocko (2000), Climate change and the collapse of the Akkadian empire: Evidence from the deep sea, *Geology*, *28*, 379–382, doi:10.1130/0091-7613(2000)28<379:CCATCO>2.0.CO;2.

da Silva, A. M., C. C. Young, and S. Levitus (Eds.) (1994), *Atlas of Surface Marine Data 1994*, vol. 1, *Algorithms and Procedures*, *NOAA Atlas NESDIS*, vol. 6, NOAA, Silver Spring, Md.

Denton, G. H., and W. Karlén (1973), Holocene climate variations: Their pattern and possible cause, *Quat. Res.*, *3*, 155–174, doi:10.1016/0033-5894(73)90040-9.

Deuser, W. G. (1968), Postdepositional changes in the oxygen isotope ratios of Pleistocene foraminifer tests in the Red Sea, *J. Geophys. Res.*, *73*, 3311–3314, doi:10.1029/JB073i010p03311.

Doose-Rolinski, H., U. Rogalla, G. Scheeder, A. Lückge, and U. von Rad (2001), High-resolution temperature and evaporation changes during the late Holocene in the northeastern Arabian Sea, *Paleoceanography*, *16*, 358–367, doi:10.1029/2000PA000511.

Edelman, Y. (1996), Reconstruction of paleoceanographic settings during the Late Holocene in the central Red Sea, M.Sc. thesis, 172 pp., Hebrew Univ., Jerusalem.

Edelman-Furstenberg, Y., A. Almogi-Labin, and C. Hemleben (2009), Palaeoceanographic evolution of the central Red Sea during the late Holocene, *Holocene*, *19*, 117–127, doi:10.1177/0959683608098955.

Ehrmann, W., G. Schmiedl, Y. Hamann, T. Kuhnt, C. Hemleben, and W. Siebel (2007), Clay minerals in the late glacial and Holocene sediments of the northern and southern Red Sea, *Palaeogeogr. Palaeoclimatol. Palaeoecol.*, *249*, 36–57, doi:10.1016/j.palaeo.2007.01.004.

Emeis, K.-C., U. Struck, H.-M. Schulz, R. Rosenberg, S. Bernasconi, H. Erlenkeuser, T. Sakamoto, and F. Martinez-Ruiz (2000), Temperature and salinity variations of Mediterranean Sea surface waters over the last 16,000 years from records of planktonic stable oxygen isotopes and alkenone unsaturation ratios, *Palaeogeogr. Palaeoclimatol. Palaeoecol.*, *158*, 259–280, doi:10.1016/S0031-0182(00)00053-5.

Eshel, G., and N. H. Naik (1997), Climatological coastal jet collision, intermediate water formation, and the general circulation of the Red Sea, *J. Phys. Oceanogr.*, *27*, 1233–1257.

Eshel, G., M. A. Cane, and M. B. Blumenthal (1994), Modes of subsurface, intermediate, and deep water renewal in the Red Sea, *J. Geophys. Res.*, *99*, 15,941–15,952, doi:10.1029/94JC01131.

Fairbanks, R. G. (1990), The age and origin of the "Younger Dryas climate event" in Greenland ice cores, *Paleoceanography*, *5*, 937–948, doi:10.1029/PA005i006p00937.

Fairbanks, R. G. (1992), Barbados sea level and Th/U ^{14}C calibration, ftp://ftp.ncdc.noaa.gov/pub/data/paleo/contributions_by_author/fairbanks1990/barbados_1990.txt, IGBP PAGES Data Contrib. Ser. 92-020, World Data Cent. for Paleoclimatol., Boulder, Colo.

Fenton, M., S. Geiselhart, E. J. Rohling, and C. Hemleben (2000), Aplanktonic zones in the Red Sea, *Mar. Micropaleontol.*, *40*, 277–294, doi:10.1016/S0377-8398(00)00042-6.

Fleitmann, D., S. J. Burns, M. Mudelsee, U. Neff, J. Kramers, A. Mangini, and A. Matter (2003), Holocene forcing of the Indian monsoon recorded in a stalagmite from southern Oman, *Science*, *300*, 1737–1739, doi:10.1126/science.1083130.

Fleitmann, D., et al. (2007), Holocene ITCZ and Indian monsoon dynamics recorded in stalagmites from Oman and Yemen (Socotra), *Quat. Sci. Rev.*, *26*, 170–188, doi:10.1016/j.quascirev.2006.04.012.

Gasse, F., and E. Van Campo (1994), Abrupt post-glacial climate events in West Asia and North Africa monsoon domains, *Earth Planet. Sci. Lett.*, *126*, 435–456, doi:10.1016/0012-821X(94)90123-6.

Geiselhart, S. (1998), Late Quaternary paleoceanographic and paleoclimatologic history of the Red Sea during the last 380.000 years: Evidence from stable isotopes and faunal assemblages, *Tueb. Mikropaläontol. Mitt.*, *17*, 1–87.

Gupta, A. K., D. M. Anderson, and J. T. Overpeck (2003), Abrupt changes in the Asian southwest monsoon during the Holocene and their links to the North Atlantic Ocean, *Nature*, *421*, 354–357, doi:10.1038/nature01340.

Hemleben, C., M. Spindler, and O. R. Anderson (1989), *Modern Planktonic Foraminifera*, 363 pp., Springer, New York.

Hemleben, C., D. Meischner, R. Zahn, A. Almogi-Labin, H. Erlenkeuser, and B. Hiller (1996), Three hundred eighty thousand year long stable isotope and faunal records from the Red Sea: Influence of global sea level change on hydrography, *Paleoceanography*, *11*, 147–156, doi:10.1029/95PA03838.

Herold, M., and G. Lohmann (2009), Eemian tropical and subtropical African moisture transport: An isotope modelling study, *Clim. Dyn.*, *33*, 1075–1088, doi:10.1007/s00382-008-0515-2.

Hopmans, E. C., S. Schouten, R. D. Pancost, M. T. J. van der Meer, and J. S. Sinninghe Damsté (2000), Analysis of intact tetraether lipids in archaeal cell material and sediments by high performance liquid chromatography/atmospheric pressure chemical ionization mass spectrometry, *Rapid Commun. Mass Spectrom.*, *14*, 585–589, doi:10.1002/(SICI)1097-0231(20000415)14:7<585::AID-RCM913>3.0.CO;2-N.

Hopmans, E. C., J. W. H. Weijers, E. Schefuss, L. Herfort, J. S. Sinninghe Damsté, and S. Schouten (2004), A novel proxy for terrestrial organic matter in sediments based on branched and isoprenoid tetraether lipids, *Earth Planet. Sci. Lett.*, *224*, 107–116, doi:10.1016/j.epsl.2004.05.012.

Hughen, K. A., et al. (2004), Marine04 marine radiocarbon age calibration, 0–26 cal kyr BP, *Radiocarbon*, *46*, 1059–1086.

Huguet, C., R. H. Smittenberg, W. Boer, J. S. Sinninghe Damsté, and S. Schouten (2007), Twentieth century proxy records of temperature and soil organic matter input in the Drammensfjord, southern Norway, *Org. Geochem.*, *38*, 1838–1849, doi:10.1016/j.orggeochem.2007.06.015.

Kennett, J. P., and B. L. Ingram (1995), A 20,000-year record of ocean circulation and climate change from the Santa Barbara Basin, *Nature*, *377*, 510–514, doi:10.1038/377510a0.

Lamy, F., H. W. Arz, G. C. Bond, A. Bahr, and J. Pätzold (2006), Multicentennial-scale hydrological changes in the Black Sea and northern Red Sea during the Holocene and the Arctic/North Atlantic Oscillation, *Paleoceanography*, *21*, PA1008, doi:10.1029/2005PA001184.

Legge, H. L., J. Mutterlose, and H. W. Arz (2006), Climatic changes in the northern Red Sea during the last 22,000 years as recorded by calcareous nannofossils, *Paleoceanography*, *21*, PA1003, doi:10.1029/2005PA001142.

Legge, H. L., J. Mutterlose, H. W. Arz, and J. Pätzold (2008), Nannoplankton successions in the northern Red Sea during the last glaciation (60 to 14.5 ka BP): Reactions to climate change, *Earth Planet. Sci. Lett.*, *270*, 271–279, doi:10.1016/j.epsl.2008.03.030.

Locke, S., and R. C. Thunell (1988), Paleoceanographic record of the last glacial/interglacial cycle in the Red Sea and Gulf of Aden, *Palaeogeogr. Palaeoclimatol. Palaeoecol.*, *64*, 163–187, doi:10.1016/0031-0182(88)90005-3.

Lückge, A., H. Doose-Rolinski, A. A. Khan, H. Schulz, and U. von Rad (2001), Monsoonal variability in the northeastern Arabian Sea during the past 5000 years: Geochemical evidence from laminated sediments, *Palaeogeogr. Palaeoclimatol. Palaeoecol.*, *167*, 273–286, doi:10.1016/S0031-0182(00)00241-8.

Malmgren, B. A., and U. Nordlund (1997), Application of artificial neural networks to paleoceanographic data, *Palaeogeogr. Palaeoclimatol. Palaeoecol.*, *136*, 359–373, doi:10.1016/S0031-0182(97)00031-X.

Manasrah, R., M. Badran, H. U. Lass, and W. Fennel (2004), Circulation and winter deep-water formation in the northern Red Sea, *Oceanologia*, *46*, 5–23.

Marchant, R., and H. Hooghiemstra (2004), Rapid environmental change in African and South American tropics around 4000 years before present: A review, *Earth Sci. Rev.*, *66*, 217–260, doi:10.1016/j.earscirev.2004.01.003.

Mawson, R., and M. A. J. Williams (1984), A wetter climate in eastern Sudan 2,000 years ago?, *Nature*, *309*, 49–51, doi:10.1038/309049a0.

Mayewski, P. A., et al. (2004), Holocene climate variability, *Quat. Res.*, *62*, 243–255, doi:10.1016/j.yqres.2004.07.001.

Morcos, S. A. (1970), Physical and chemical oceanography of the Red Sea, *Oceanogr. Mar. Biol.*, *8*, 73–202.

Murray, S. P., and W. Johns (1997), Direct observations of seasonal exchange through the Bab el Mandab Strait, *Geophys. Res. Lett.*, *24*, 2557–2560, doi:10.1029/97GL02741.

Naidu, P. D., and B. A. Malmgren (1996), A high-resolution record of late Quaternary upwelling along the Oman Margin, Arabian Sea based on planktonic foraminifera, *Paleoceanography*, *11*, 129–140, doi:10.1029/95PA03198.

Naqvi, W. A., and R. G. Fairbanks (1996), A 27,000 year record of Red Sea outflow: Implication for timing of post-glacial monsoon intensification, *Geophys. Res. Lett.*, *23*, 1501–1504, doi:10.1029/96GL01030.

Niemi, T. M., H. Zhang, M. Atallah, and J. B. J. Harrison (2001), Late Pleistocene and Holocene slip rate of the northern Wadi Araba fault, Dead Sea Transform, Jordan, *J. Seismol.*, *5*, 449–474, doi:10.1023/A:1011487912054.

O'Brien, S. R., P. A. Mayewski, L. D. Meeker, D. A. Meese, M. S. Twickler, and S. I. Whitlow (1995), Complexity of Holocene climate as reconstructed from a Greenland ice core, *Science*, *270*, 1962–1964, doi:10.1126/science.270.5244.1962.

Overpeck, J., D. Anderson, S. Trumbore, and W. Prell (1996), The southwest Indian monsoon over the last 18 000 years, *Clim. Dyn.*, *12*, 213–225, doi:10.1007/BF00211619.

Parker, A. G., A. S. Goudie, S. Stokes, K. White, M. J. Hodson, M. Manning, and D. Kennet (2006), A record of Holocene climate change from lake geochemical analyses in southeastern Arabia, *Quat. Res.*, *66*, 465–476, doi:10.1016/j.yqres.2006.07.001.

Patzert, W. C. (1974), Seasonal reversal in Red Sea circulation, in *L'Oceanographie Physique de la Mer Rouge*, pp. 55–89, CNEXO, Saclay, France.

Pedgley, D. E. (1974), An outline of the weather and climate of the Red Sea, in *L'Oceanographie Physique de la Mer Rouge*, pp. 9–27, CNEXO, Saclay, France.

Petite-Maire, N., L. Beufort, and N. Page (1997), Holocene climate change and man in the present day Sahara Desert, in *Third Millennium BC Climate Change and Old World Collapse*, *NATO ASI Ser., Ser. I*, vol. 49, edited by H. N. Dalfes, G. Kukla, and H. Weiss, pp. 297–308, Springer, Berlin.

Phadtare, N. R. (2000), Sharp decrease in summer monsoon strength 4000–3500 cal yr B.P. in the Central Higher Himalaya of India based on pollen evidence from alpine peat, *Quat. Res.*, *53*, 122–129, doi:10.1006/qres.1999.2108.

Quadfasel, D., and H. Baudner (1993), Gyre-scale circulation cells in the Red Sea, *Oceanol. Acta*, *16*, 221–229.

Reimer, P. J., and R. W. Reimer (2001), A marine reservoir correction database and on-line interface, *Radiocarbon*, *43*, 461–463.

Rimbu, N., G. Lohmann, S. J. Lorenz, J. H. Kim, and R. R. Schneider (2004), Holocene climate variability as derived from alkenone sea surface temperature and coupled ocean-atmosphere model experiments, *Clim. Dyn.*, *23*, 215–227, doi:10.1007/s00382-004-0435-8.

Rohling, E. J. (1999), Environmental control on Mediterranean salinity and $\delta^{18}O$, *Paleoceanography*, *14*, 706–715, doi:10.1029/1999PA900042.

Rohling, E. J., and H. Pälike (2005), Centennial-scale climate cooling with a sudden cold event around 8,200 years ago, *Nature*, *434*, 975–979, doi:10.1038/nature03421.

Rohling, E. J., M. Fenton, F. J. Jorissen, P. Bertrand, G. Ganssen, and J. P. Caulet (1998), Magnitudes of sea-level lowstands of the past 500,000 years, *Nature*, *394*, 162–165, doi:10.1038/28134.

Rohling, E. J., P. A. Mayewski, R. H. Abu-Zied, J. S. L. Casford, and A. Hayes (2002), Holocene atmosphere-ocean interactions: Records from Greenland and the Aegean Sea, *Clim. Dyn.*, *18*, 587–593, doi:10.1007/s00382-001-0194-8.

Rohling, E. J., K. Grant, C. Hemleben, M. Kucera, A. P. Roberts, I. Schmeltzer, H. Schulz, M. Siccha, M. Siddall, and G. Trommer (2008a), New constraints on the timing of sea level fluctuations during early to middle marine isotope stage 3, *Paleoceanography*, *23*, PA3219, doi:10.1029/2008PA001617.

Rohling, E. J., K. Grant, C. Hemleben, M. Siddall, B. A. A. Hoogakker, M. Bolshaw, and M. Kucera (2008b), High rates of sea-level rise during the last interglacial period, *Nat. Geosci.*, *1*, 38–42, doi:10.1038/ngeo.2007.28.

Sarkar, A., R. Ramesh, B. L. K. Somayajulu, R. Agnihotri, A. J. T. Jull, and G. S. Burr (2000), High resolution Holocene monsoon record from the eastern Arabian Sea, *Earth Planet. Sci. Lett.*, *177*, 209–218, doi:10.1016/S0012-821X(00)00053-4.

Schilman, B., M. Bar-Matthews, A. Almogi-Labin, and B. Luz (2001), Global climate instability reflected by eastern Mediterranean marine records during the late Holocene, *Palaeogeogr. Palaeoclimatol. Palaeoecol.*, *176*, 157–176, doi:10.1016/S0031-0182(01)00336-4.

Schmelzer, I. (1998), High-frequency event-stratigraphy and paleoceanography of the Red Sea, Ph.D. thesis, 124 pp., Univ. of Tübingen, Tübingen, Germany.

Schouten, S., E. C. Hopmans, E. Schefuss, and J. S. Sinninghe Damsté (2002), Distributional variations in marine crenarchaeotal membrane lipids: A new tool for reconstructing ancient sea water temperatures?, *Earth Planet. Sci. Lett.*, *204*, 265–274, doi:10.1016/S0012-821X(02)00979-2.

Schouten, S., C. Huguet, E. C. Hopmans, M. V. M. Kienhuis, and J. S. Sinninghe Damsté (2007), Analytical methodology for TEX_{86} paleothermometry by high-performance liquid chromatography/atmospheric pressure chemical ionization-mass spectrometry, *Anal. Chem.*, *79*, 2940–2944, doi:10.1021/ac062339v.

Seeberg-Elverfeldt, I. A., C. B. Lange, J. Pätzold, and G. Kuhn (2005), Laminae type and possible mechanisms for the formation of laminated sediments in the Shaban Deep, northern Red Sea, *Ocean Sci.*, *1*, 113–126, doi:10.5194/os-1-113-2005.

Siccha, M., G. Trommer, H. Schulz, C. Hemleben, and M. Kucera (2009), Factors controlling the distribution of planktonic foraminifera in the Red Sea and implications for paleoenvironmental reconstructions by transfer functions, *Mar. Micropaleontol.*, *72*, 146–156, doi:10.1016/j.marmicro.2009.04.002.

Siddall, M., D. A. Smeed, S. Matthiesen, and E. J. Rohling (2002), Modelling the seasonal cycle of the exchange flow in Bab El Mandab (Red Sea), *Deep Sea Res., Part I*, *49*, 1551–1569, doi:10.1016/S0967-0637(02)00043-2.

Siddall, M., E. J. Rohling, A. Almogi-Labin, C. Hemleben, D. Meischner, I. Schmelzer, and D. A. Smeed (2003), Sea-level fluctuations during the last glacial cycle, *Nature*, *423*, 853–858, doi:10.1038/nature01690.

Siddall, M., D. A. Smeed, C. Hemleben, E. J. Rohling, I. Schmelzer, and W. Peltier (2004), Understanding the Red Sea response to sea level, *Earth Planet. Sci. Lett.*, *225*, 421–434, doi:10.1016/j.epsl.2004.06.008.

Smeed, D. A. (1997), Seasonal variation of the flow in the strait of Bab al Mandab, *Oceanol. Acta*, *20*, 773–781.

Smeed, D. A. (2004), Exchange through the Bab el Mandab, *Deep Sea Res., Part II*, *51*, 455–474, doi:10.1016/j.dsr2.2003.11.002.

Sofianos, S. S., and W. E. Johns (2001), Wind induced sea level variability in the Red Sea, *Geophys. Res. Lett.*, *28*, 3175–3178, doi:10.1029/2000GL012442.

Sofianos, S. S., and W. E. Johns (2002), An oceanic general circulation model (OGCM) investigation of the Red Sea circulation: 1. Exchange between the Red Sea and the Indian Ocean, *J. Geophys. Res.*, *107*(C11), 3196, doi:10.1029/2001JC001184.

Sofianos, S. S., and W. E. Johns (2003), An oceanic general circulation model (OGCM) investigation of the Red Sea circulation: 2. Three-dimensional circulation in the Red Sea, *J. Geophys. Res.*, *108*(C3), 3066, doi:10.1029/2001JC001185.

Sofianos, S. S., W. E. Johns, and S. P. Murray (2002), Heat and freshwater budgets in the Red Sea from direct observations at Bab el Mandeb, *Deep Sea Res., Part II*, *49*, 1323–1340, doi:10.1016/S0967-0645(01)00164-3.

Souvermezoglou, E., N. Metzl, and A. Poisson (1989), Red Sea budgets of salinity, nutrients and carbon calculated in the Strait of Bab-El-Mandab during the summer and winter seasons, *J. Mar. Res.*, *47*, 441–456, doi:10.1357/002224089785076244.

Staubwasser, M., and H. Weiss (2006), Holocene climate and cultural evolution in late prehistoric-early historic West Asia, *Quat. Res.*, *66*, 372–387, doi:10.1016/j.yqres.2006.09.001.

Staubwasser, M., F. Sirocko, P. M. Grootes, and M. Segl (2003), Climate change at the 4.2 ka BP termination of the Indus valley civilization and Holocene South Asian monsoon variability, *Geophys. Res. Lett.*, *30*(8), 1425, doi:10.1029/2002GL016822.

Stuiver, M., and P. J. Reimer (1993), Extended ^{14}C data base and revised Calib 3.0 ^{14}C age calibration program, *Radiocarbon*, *35*, 215–230.

ter Braak, C. J. F., and S. Juggins (1993), Weighted averaging partial least squares regression (WA-PLS): An improved method for reconstructing environmental variables from species assemblages, *Hydrobiologia*, *269–270*, 485–502, doi:10.1007/BF00028046.

Thompson, L. G., et al. (2002), Kilimanjaro ice core records: Evidence of Holocene climate change in tropical Africa, *Science*, *298*, 589–593, doi:10.1126/science.1073198.

Trommer, G. (2009), Development, validation and application of new paleoceanographical techniques for the reconstruction of past climate conditions in the Red Sea, Ph.D. thesis, 128 pp., Univ. of Tübingen, Tübingen, Germany.

Trommer, G., M. Siccha, M. T. J. van der Meer, S. Schouten, J. S. Sinninghe Damsté, H. Schulz, C. Hemleben, and M. Kucera (2009), Distribution of Crenarchaeota tetraether membrane lipids in surface sediments from the Red Sea, *Org. Geochem.*, *40*, 724–731, doi:10.1016/j.orggeochem.2009.03.001.

Veldhuis, M. J. W., G. W. Kraay, J. D. L. Van Bleijswijk, and M. A. Baars (1997), Seasonal and spatial variability in phytoplankton biomass, productivity and growth in the northwestern Indian Ocean: The southwest and northeast monsoon, 1992–1993, *Deep Sea Res., Part I*, *44*, 425–449, doi:10.1016/S0967-0637(96)00116-1.

von Rad, U., A. Lückge, W. H. Berger, and H. Doose-Rolinski (2006), Annual to millennial monsoonal cyclicity recorded in Holocene varved sediments from the NE Arabian Sea, *J. Geol. Soc. India*, *68*, 353–368.

Walsh, E. M., A. E. Ingalls, and R. G. Keil (2008), Sources and transport of terrestrial organic matter in Vancouver Island fjords and the Vancouver-Washington Margin: A multiproxy approach using $d^{13}C_{org}$, lignin phenols, and the ether lipid BIT index, *Limnol. Oceanogr.*, *53*, 1054–1063.

Weijers, J. W. H., S. Schouten, O. C. Spaargaren, and J. S. Sinninghe Damsté (2006), Occurrence and distribution of tetraether membrane lipids in soils: Implications for the use of the TEX_{86} proxy and the BIT index, *Org. Geochem.*, *37*, 1680–1693, doi:10.1016/j.orggeochem.2006.07.018.

Weikert, H. (1987), Plankton and the pelagic environment, in *Red Sea (Key Environments)*, edited by F. J. Edwards and S. M. Head, pp. 90–111, Pergamon, New York.

Winter, A. (1982), Paleoenvironmental interpretation of Quaternary coccolith assemblages from the Gulf of Aqaba (Elat), Red Sea, *Rev. Esp. Micropaleontol.*, *14*, 291–314.

Woelk, S., and D. Quadfasel (1996), Renewal of deep water in the Red Sea during 1982–1987, *J. Geophys. Res.*, *101*, 18,155–18,165, doi:10.1029/96JC01148.

K. Grant and E. J. Rohling, National Oceanography Centre, University of Southampton, Southampton SO14 3ZH, UK.

C. Hemleben and M. Kucera, Institute of Geosciences, University of Tübingen, D-72076 Tübingen, Germany.

S. Schouten and M. T. J. van der Meer, Department of Marine Organic Biogeochemistry, Royal Netherlands Institute for Sea Research, NL-1790 AB Den Burg, Netherlands.

M. Siccha, Laboratoire des Bio-Indicateurs Actuels et Fossiles, UFR Sciences, F-49045 Angers, France.

G. Trommer, Europole Mer, European Institute for Marine Studies, Technopole Brest-Iroise, F-29280 Plouzane, France. (trommer@univ-brest.fr)